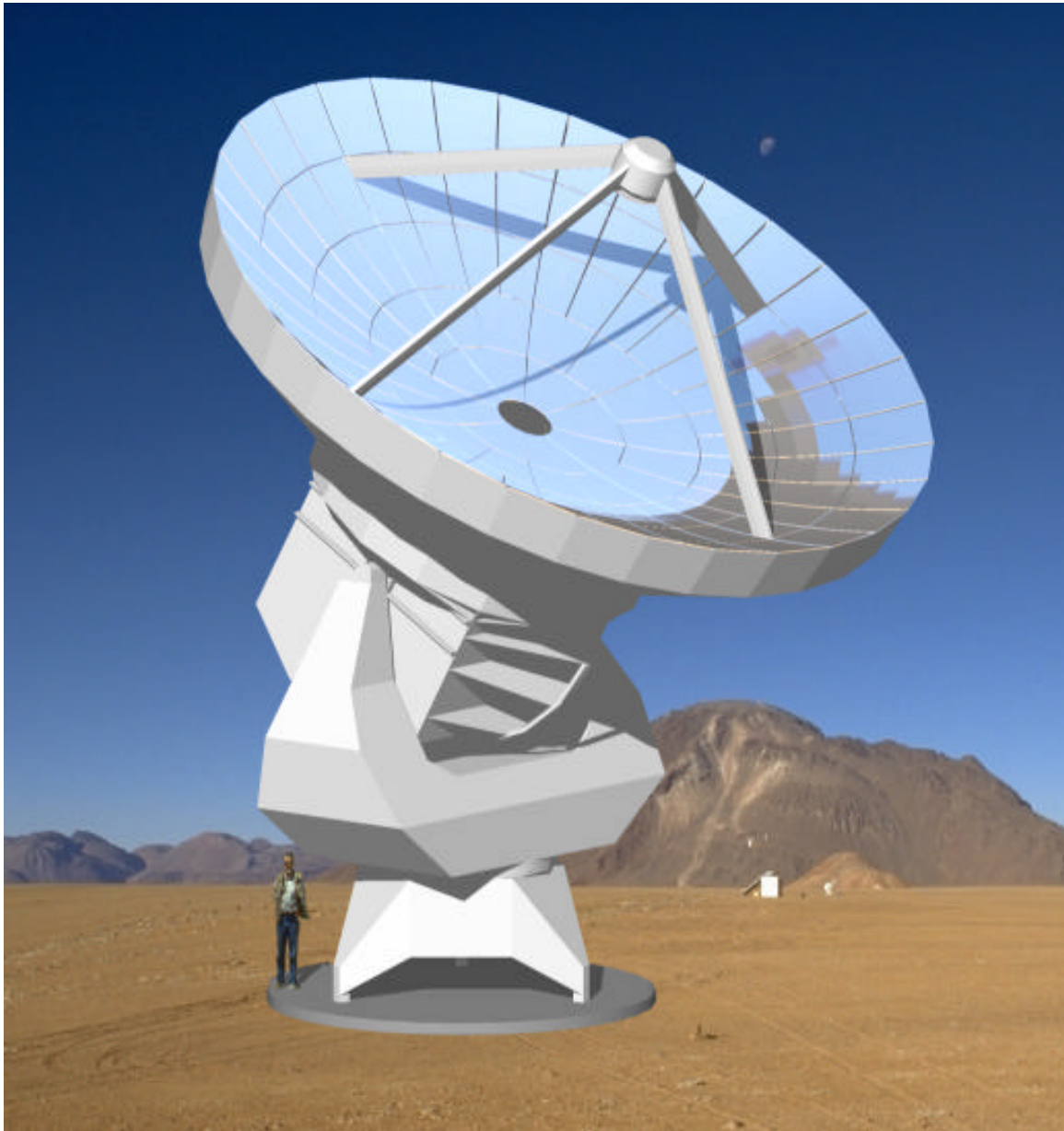


A 10-m Antenna Design for the Millimeter Array



J. Lugten¹, J. Kingsley¹, J. Cheng¹, V. Gasho¹, and M. Fleming²

¹National Radio Astronomy Observatory

²Berkeley Illinois Maryland Association

FEBRUARY 1999



NATIONAL RADIO ASTRONOMY OBSERVATORY

A facility of the National Science Foundation operated under cooperative agreement by Associated Universities, Inc.

NATIONAL RADIO ASTRONOMY OBSERVATORY

949 North Cherry Avenue
Campus Building 65
Tucson, Arizona 85721-0655

John B. Lugten	N.R.A.O.	jlugten@nrao.edu
Jeffrey S. Kingsley	N.R.A.O.	jkingsle@nrao.edu
Jingquan Cheng	N.R.A.O.	jcheng@nrao.edu
Victor L. Gasho	N.R.A.O.	vgasho@nrao.edu
Matt Fleming	B.I.M.A.	mflaming@astron.berkeley.edu

Cover: Artist's conception of this antenna design on the Chajnantor, Chile site.

*Photograph by Simon Radford.
Rendering by Victor Gasho.*

ABSTRACT

A design is presented for a 10-m diameter millimeter and sub-millimeter wavelength radio telescope which is suitable for the Millimeter Array project. The telescope features very high accuracy, light weight, cast aluminum primary mirror panels that are machined only on their front surfaces and are supported by an all carbon fiber reinforced plastic (CFRP) supporting structure. The aluminum secondary mirror is supported by a high modulus CFRP quadripod. The equivalent surface accuracy is less than 17 micrometers RMS including effects of gravity, wind loading, and thermal effects. A large cabin is available for receivers and other antenna systems. The mount is an elevation-over-azimuth design constructed from welded steel plate. The mount uses novel techniques to measure the dish orientation; a non-load bearing reference structure, in combination with displacement sensors and tiltmeters measures the deflection of the major mount and foundation elements due to wind and thermal loading of the structure. Sub-arcsecond pointing accuracy is expected for most observing conditions at the proposed Millimeter Array site. The antenna is driven by extremely stiff, zero-backlash friction drives with a single speed reduction. Special care is taken to assure that the azimuth bearing remains flat in order to minimize a common antenna problem which is that the azimuth axis tilts with changes in azimuth angle. The base of the antenna interfaces to the foundation at only 3 points to provide kinematic support of the antenna. The 3-point support allows very rapid relocation of an antenna to a different foundation; adjustable interfaces are provided on all foundations and antennas to allow everything to be pre-leveled. A transporter design is presented which has a wide track for stability yet is highly maneuverable as required for rapid antenna access in the most compact array configuration.

This design can be improved by further optimization, mainly in the yoke and cabin. Higher resonant frequencies, improved pointing accuracy near zenith, and smaller surface error due to gravitational load are expected. Some possible approaches to scaling the design to a 12-meter aperture are discussed.

TABLE OF CONTENTS

1. Introduction	1
2. Specifications	2
3. Antenna Design	3
3.1 Optical Design.....	3
3.1.1 Optical Configuration	3
3.1.2 Low Noise.....	3
3.1.3 Close Packing.....	5
3.1.4 Solar Observing	5
3.2 Mechanical Design.....	5
3.2.1 Primary Mirror Backup Structure	7
3.2.2 Panels.....	9
3.2.3 Apex Structur	11
3.2.4 Receiver Cabin.....	11
3.2.5 Yoke.....	12
3.2.6 Base.....	13
3.2.7 Bearings	14
3.2.8 Drives.....	15
3.2.9 Cable Wrap.....	16
3.2.10 Thermal Control.....	17
3.3 Foundation	17
3.4 Control System.....	19
4. Antenna Metrology	21
4.1 Independent Reference Arms.....	21
4.2 Tiltmeters.....	22
4.3 Optical Pointing Telescope.....	23
4.4 Temperature Probes.....	23
5. Antenna Performance	25
5.1 Surface Error Budget.....	26

5.2 Optomechanical Performance.....	27
5.2.1 FEA Model Description and Structural Analysis.....	27
5.2.2 Gravity Load.....	28
5.2.3 Wind Load.....	30
5.2.4 Thermal Load.....	33
5.2.5 Path Length Errors.....	35
5.2.6 Modal Analysis.....	35
5.2.7 Dynamic Performance.....	37
6. Antenna Handling.....	39
6.1 Transporter.....	40
6.2 Receiver Service Vehicle.....	41
6.3 Assembly and Maintenance	42
7. Conclusion.....	45
8. Appendix A: Antenna Drawings.....	47
9. Appendix B: Locked Rotor Resonance Frequencies.....	59
10. Appendix C: Control System Outline.....	61
11. Acknowledgments.....	63
12. References.....	65

1. INTRODUCTION

The 10 meter diameter antenna described here was designed to meet the performance requirements for the Millimeter Array project. It has been designed with antenna performance foremost. The major antenna performance goals were excellent pointing accuracy, surface accuracy, dynamic performance and path length stability, with the ability to pack antennas closely without a possibility of collision, low antenna noise, low manufacturing cost, low weight, and low maintenance. Only a few significant compromises were made to accommodate the requirements of integrating the antenna into the entire instrument. The three main competing goals which adversely affected antenna performance were choosing a large receiver cabin, choosing a compact antenna base to allow for a small maneuverable transporter, and choosing adjustable antenna legs and foundations to allow rapid placement of the antenna at each foundation.

We believe this design meets the antenna performance requirements for the Millimeter Array.

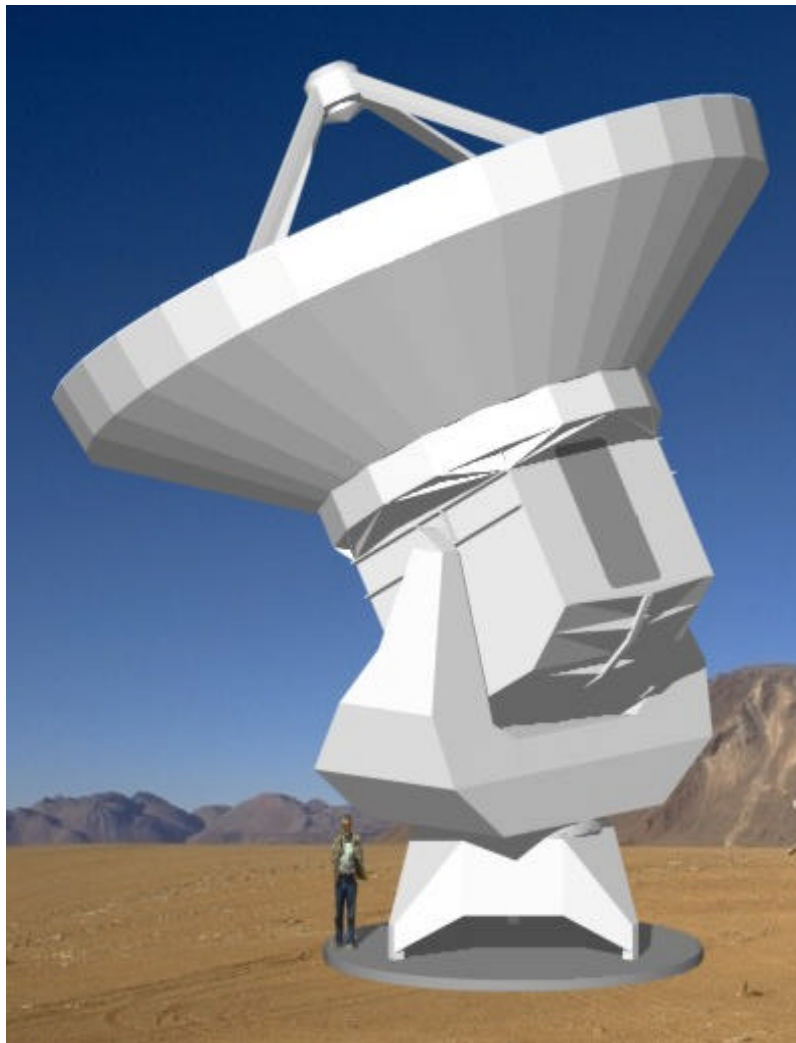


Figure 1-1. NRAO 10 meter antenna rendering.

2. SPECIFICATIONS

The specifications of the MMA antennas have evolved in order to meet the scientific goals of the project. Since this report was written, the antenna aperture and pointing specifications have changed. Listed below in Table 2.1-1 are the specifications for this antenna design.

ITEM	SPECIFICATION	NOTES
Site	Chajnantor, Chile	5060 meters elevation, volcanic soil
Antennas	36	Transportable on rubber tire vehicle
Aperture	10 meters	Minimal blockage
Frequency Range	30 GHz - 900 GHz	
Surface Accuracy	25 μ m rms	Total system
Pointing accuracy (9 m/s wind, 30 min. between calibration)	1/30 Beamwidth at 300 GHz, rms (0.8 arcsec.)	
Phase Stability	15 micron rms	Median wind conditions
Close Packing	1.25 * Diameter = 12.5 meters	
Fast Switching	Move 1.5 E. On sky in 1.5 seconds @ 3" pointing	
Maximum Velocity	3 E/sec, 6 E/sec	Elevation and azimuth respectively
Maximum Acceleration	12E/sec ² , 24 E/sec ²	Elevation and azimuth respectively
Lowest Resonant Frequency	>8 Hz	
Azimuth Range	+/- 270E from North	
Elevation Range	0E to 125E	
Configuration	Elevation-over-azimuth mount, Cassegrain focus	
Subreflector	3 Beamwidths @ 86 GHz	Nutation
Solar Observing	Allowed	
Maximum Wind Speed	65 meters/sec	Survival
Design Wind Speed	9 meters /sec	Evaluation of specifications
Foundations	180	
Receiver Cabin Size	3 meters x 3 meters x 2.6 meters	Rectangular shape
Cabin Door Size	1 meter x 2 meters	

Table 2.1-1. Antenna design specifications.

3. ANTENNA DESIGN

3.1 OPTICAL DESIGN

A Cassegrain geometry with a symmetric main reflector has been chosen as the optical design for the Millimeter Array antenna because it is a simple, low-noise design. Feeds for the various frequency bands are located off-axis in the Cassegrain focal plane [1][2][3]. Care is taken to minimize the volume swept by the moving dish in order to achieve good close packing performance of the antennas [4]. The surface of the primary and secondary mirrors are made to scatter solar radiation to allow observations of the sun and sources near the sun, without overheating the secondary mirror or the receiver.

3.1.1 OPTICAL CONFIGURATION

The optical configuration is shown in Figure 3.1.1-1, which also lists the key parameters. The size of the secondary is as small as possible to accommodate the required receiver feeds in the Cassegrain focal plane. The geometrical blockage by the secondary is 0.58%, and that of the quadripod is 2.08%, for a total geometrical blockage of 2.66%. The nutation performance of this size subreflector has not been studied in detail.

3.1.2 LOW NOISE

The Cassegrain geometry can provide very low antenna noise; it is better than prime focus geometries because illumination spillover falls onto the cold sky rather than warm ground, and it avoids any additional losses by having not more than 2 reflectors. By placing the feeds in the Cassegrain focal plane, additional reflectors and their associated resistive, scattering, and spillover losses are avoided. Another element in minimizing antenna noise is to minimize the total radiation scattered by the quadripod into the receiver feeds. The inner surfaces of the support legs pass as far outboard of the secondary mirror as possible and the base of the legs are placed rather far from the center of the primary mirror. This results in minimizing the total area of the dish which is shadowed either by the interception of the spherical wave passing between the primary and secondary mirrors or of the plane wave passing between the primary and the sky. The final element of low noise performance is to assure that the light which is scattered by the quadripod legs into the receivers originates on the cold sky rather than the warm ground. A scatter cone in the center of the secondary assures that light from the center of the illumination pattern (the part blocked by the secondary mirror's shadow on the primary) originates on the sky a few degrees away from the primary beam, after reflection off the primary. Light blocked by the quadripod legs is scattered directly to the sky about 20 degrees away from the primary beam by V-shaped reflectors which enclose the structural elements. An alternative possibility for the quadripod leg scattering, which may be superior, is to use flat-bottomed (rather than V-shaped) reflectors around the legs; this reflects light first to the primary mirror then onto the sky [4] [5] [6]. With this second approach, the scattered light is terminated on a larger region of sky, further from the primary beam. Also, the cross sectional area

of the leg is only about half that of the V-shaped reflectors, which reduces wind loading on the support structure considerably. Based partly on the experience at BIMA , the expected system noise contribution of the antenna is less than about 6 K [5].

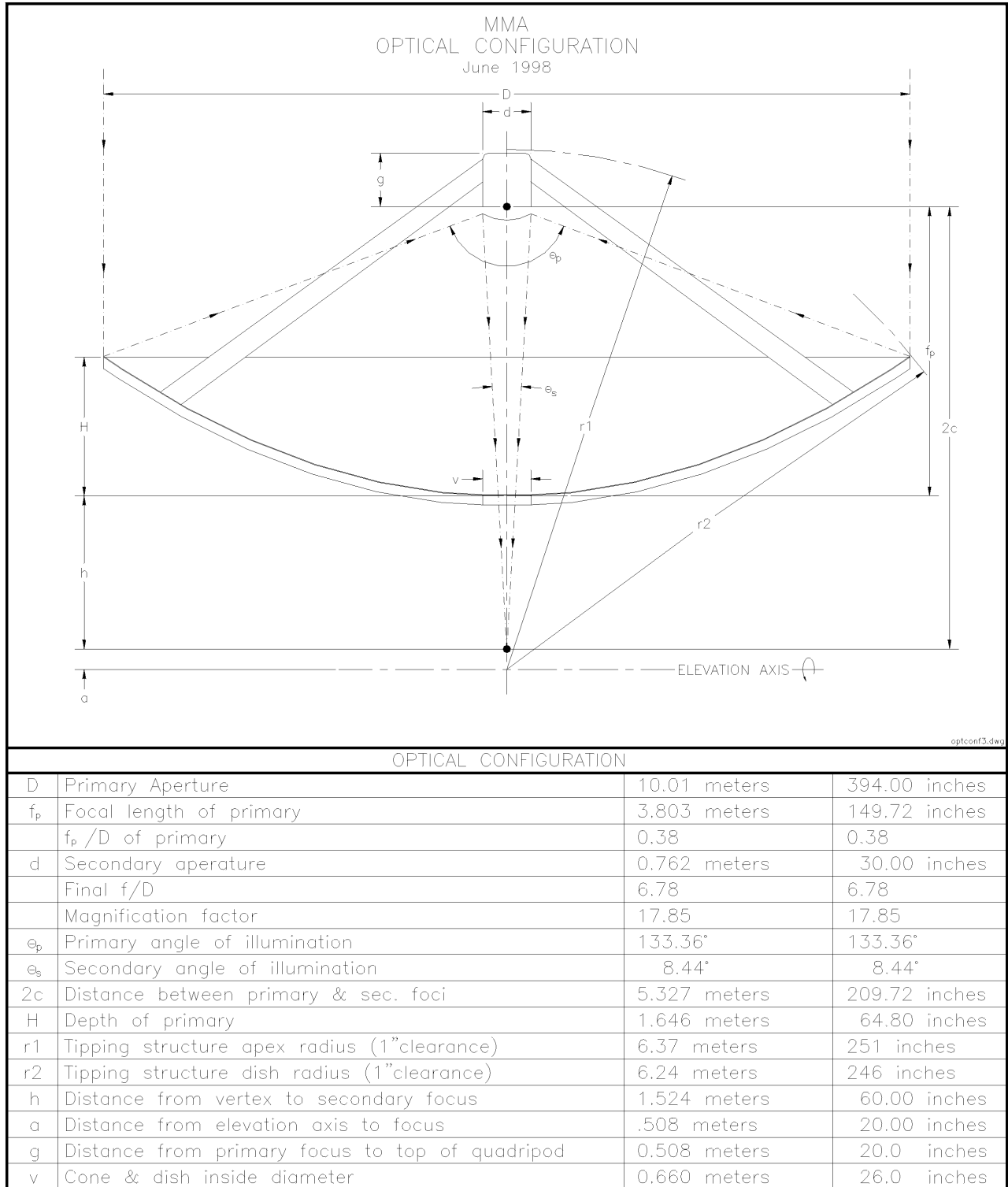


Figure 3.1.1-1. Optical layout of antenna.

3.1.3 CLOSE PACKING

As the telescope dish is moved, the edge of the dish sweeps out a sphere whose radius is the distance from the intersection of the elevation and azimuth axes to the edge of the primary mirror, r_2 . Likewise, the secondary drive housing sweeps out a sphere of radius r_1 . As listed in Figure 3.1.1-1, $r_1/r_{dish} = 1.27$ and $r_2/r_{dish} = 1.25$, allowing about 2 cm of clearance. Adjacent antennas can be placed as close as 12.5 meters with no possibility of collision for all elevations above 14 degrees, and as close as 12.7 meters with no possibility of collision for any elevation. On a newer design, the closest spacing with no possibility of collision for any elevation has been reduced to less than 12.5 meters.

3.1.4 SOLAR OBSERVING

Solar observations and observations of sources close to the sun are possible by using primary and secondary reflector surfaces which scatter solar energy sufficiently to avoid overheating the secondary mirror and the receiver cabin window. With the machined aluminum panels used in this design, the scattering may be achieved simply by the final machining process used. Alternatively, a chemical process such as anodization could be used to obtain a surface which scatters sunlight. Scattering from the primary mirror must be sufficient to cause less than about 5% of light of 5 microns wavelength or less to hit the secondary. If the secondary has the same roughness, then less than 200 Watts enter the receiver cabin.

3.2 MECHANICAL DESIGN

The overall design of the antenna is shown in Figure 3.2-1.

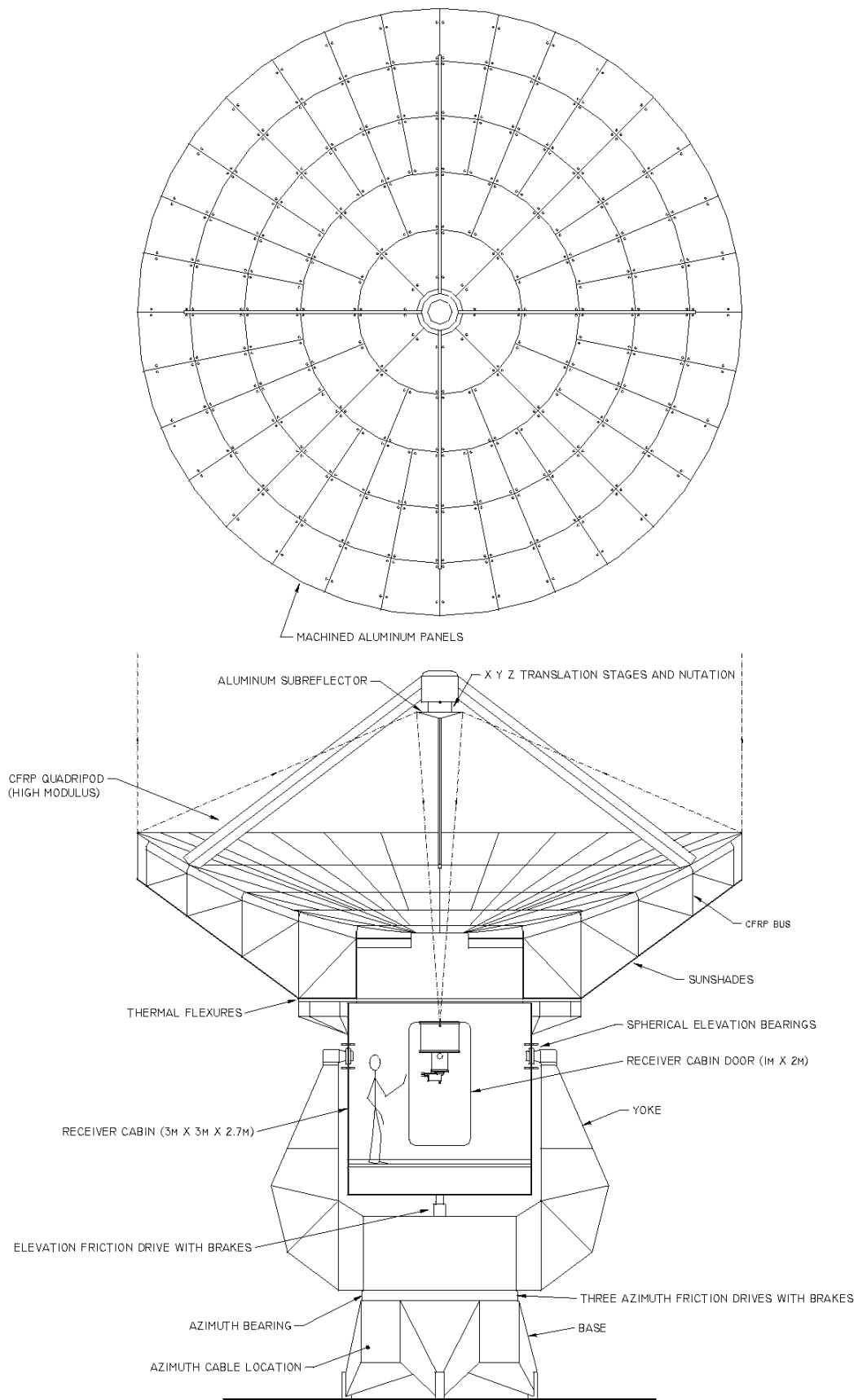


Figure 3.2-1. A 10 meter antenna design.

3.2.1 PRIMARY MIRROR BACKUP STRUCTURE

The primary mirror backup structure (BUS) is made entirely of carbon fiber reinforced plastic (CFRP). Radial trusses emanate from a central hub and are interconnected by circumferential members and diagonals as shown in Figures 3.2.1-1, 3.2.1-2, and 3.2.1-3. The key to avoiding metal in the entire BUS is to find a suitable geometry for bonding the joints between the CFRP elements [9]. For the geometry used here, each radial truss is a planar structure and the truss elements connecting to a particular joint are aligned so that the neutral axes of all elements intersect at a single point, thus avoiding all secondary bending. The neutral axes of the circumferential members also intersect at each joint, but the circumferential element joints are not coincident with the radial element joints.

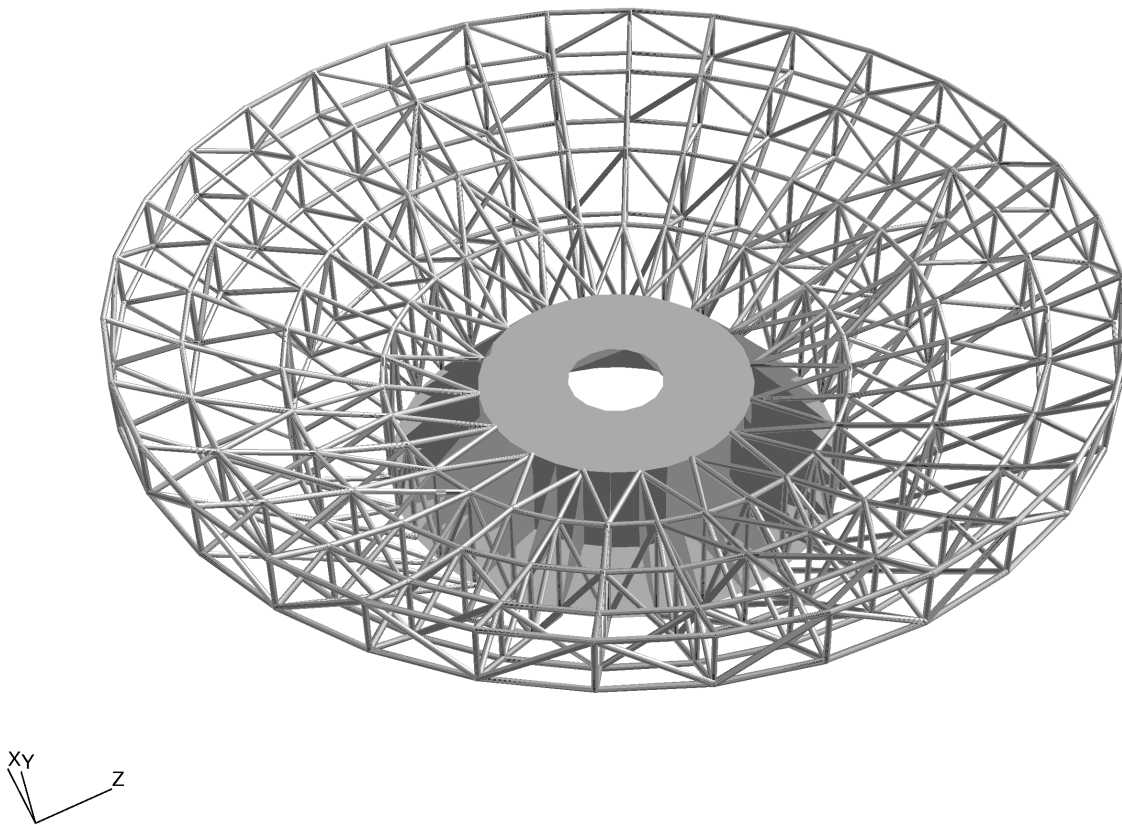


Figure 3.2.1-1 BUS FEA model.

Truss elements consist of a pair of back-to-back angle sections which are connected to other elements by bonding the inner faces to a CFRP gusset plate as shown in Figure 3.2.1-3. The angle sections have mostly uniaxial fibers resulting in a very low coefficient of thermal expansion (CTE) (about 1 ppm/C), and can probably be made by the pultrusion process. The plate elements of the central hub and gussets are a quasi-isotropic material; these elements must have a high content of perhaps a higher quality fiber in order to have a comparably low CTE.

Besides achieving a very low CTE using mostly low cost CFRP, the design has a number of other advantages. The simple geometry of the joints provides very large shear-loaded bonds, while accommodating very coarse dimensional tolerances for the lengths of the angle sections. Using back-to-back angles rather than tube has the advantage that bond areas are easily accessible and bond pressure is easily applied. Variations in the gusset thickness do not affect the bond thickness. Possible areas of concern might be compatibility problems between the resins used in the pultruded elements and in the other elements. Also, it is desirable to have some non-axial fibers in the pultruded sections; this can be done, but often is not.

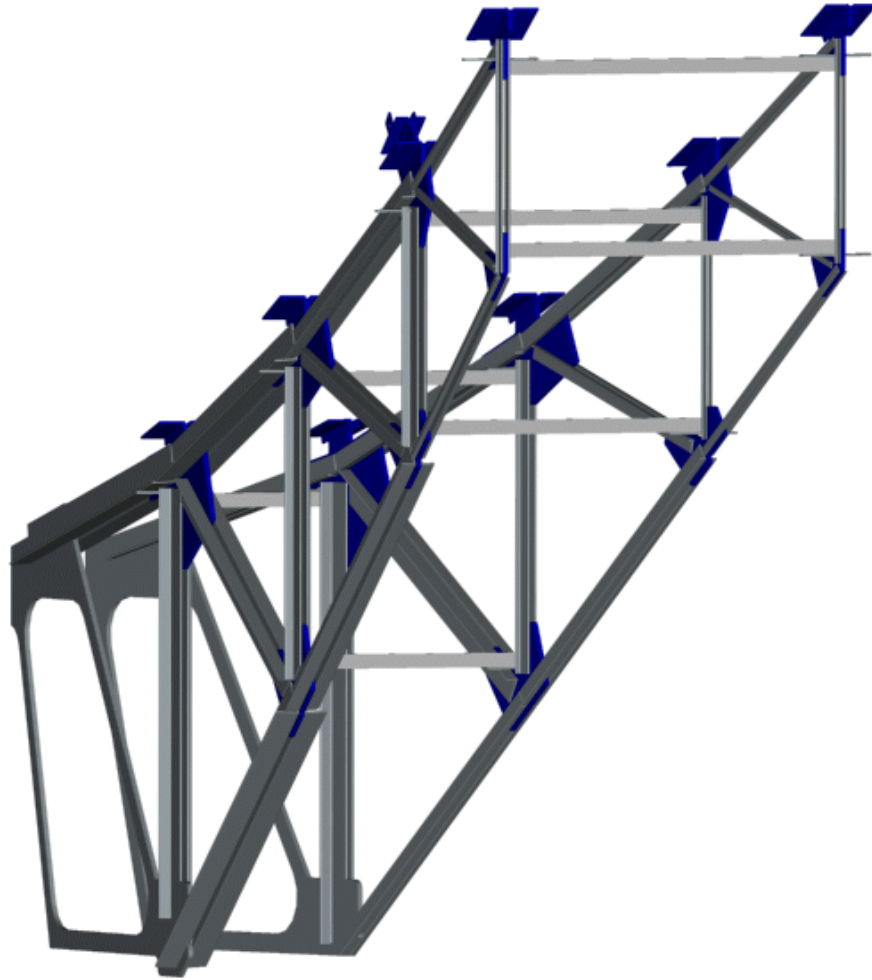


Figure 3.2.1-2. Two radial trusses of the BUS.

Because the structure is entirely CFRP, including the joints, it has a far lower mass and overall CTE than if it contained steel node type joints. With metal nodes, the weight of the nodes is typically comparable to that of the CFRP, so the total weight is roughly twice that of the all CFRP design. Unless the metal nodes are invar the overall CTE is dominated by the metal.

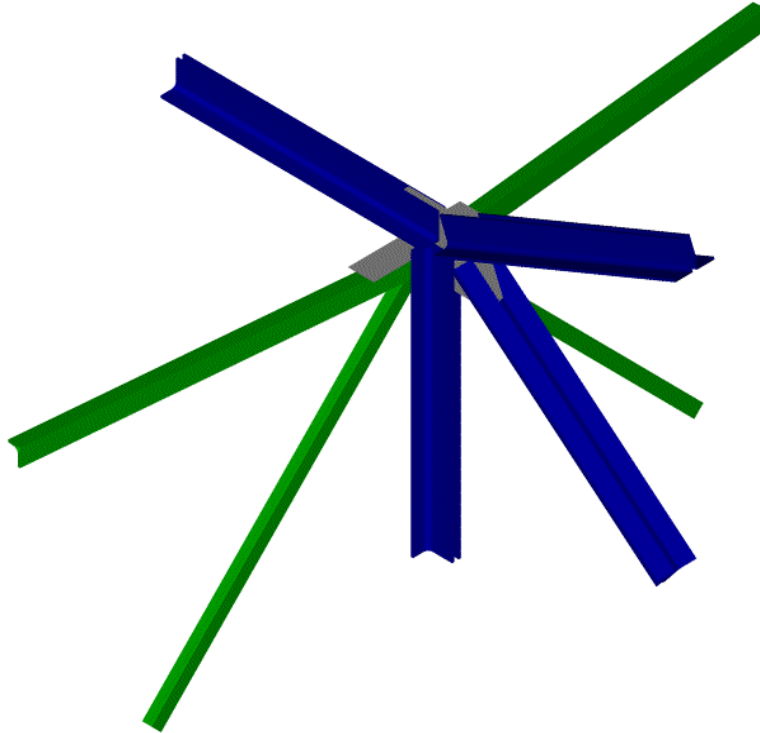


Figure 3.2.1-3. Typical BUS connection joint.

3.2.2 PANELS

The panels of the primary mirror are aluminum castings which are machined on the front surface and have four mounting points as shown in Figure 3.2.2-1. Typically, the casting is expected to have 3-millimeter wall thickness on the stiffening ribs and front skin before machining, which is routinely achieved by using a proprietary method known as V-process casting [7]. The maximum dimensions of the panels are typically 1 meter or less. This modest size is expected to result in a very low manufacturing cost due to the common availability of machining centers with our desired accuracy and work volume. Another key advantage of the modest panel size is that panel curvature due to temperature gradients through the thickness, caused by solar heating of the front surface, contributes only about 4 microns rms to the surface error budget [8].

Gravitational and wind loading produce minor contributions to the error budget. The choice of straight ribs in a rectangular geometry, as shown in Figure 3.2.2-2, is key to achieving the desired panel stiffness. With this rib geometry, the panel can be conveniently supported at its four corners. Although the panel is over-constrained in principle, this rib pattern produces a panel which is so soft in torsion that a normal force of less than 0.1 N applied at one corner will lift that corner by 1 micron, while the other 3 corners are simply supported. The panel and adjusters were modeled at an average weight of 20 kg/m²; however, the final panels may weigh less.

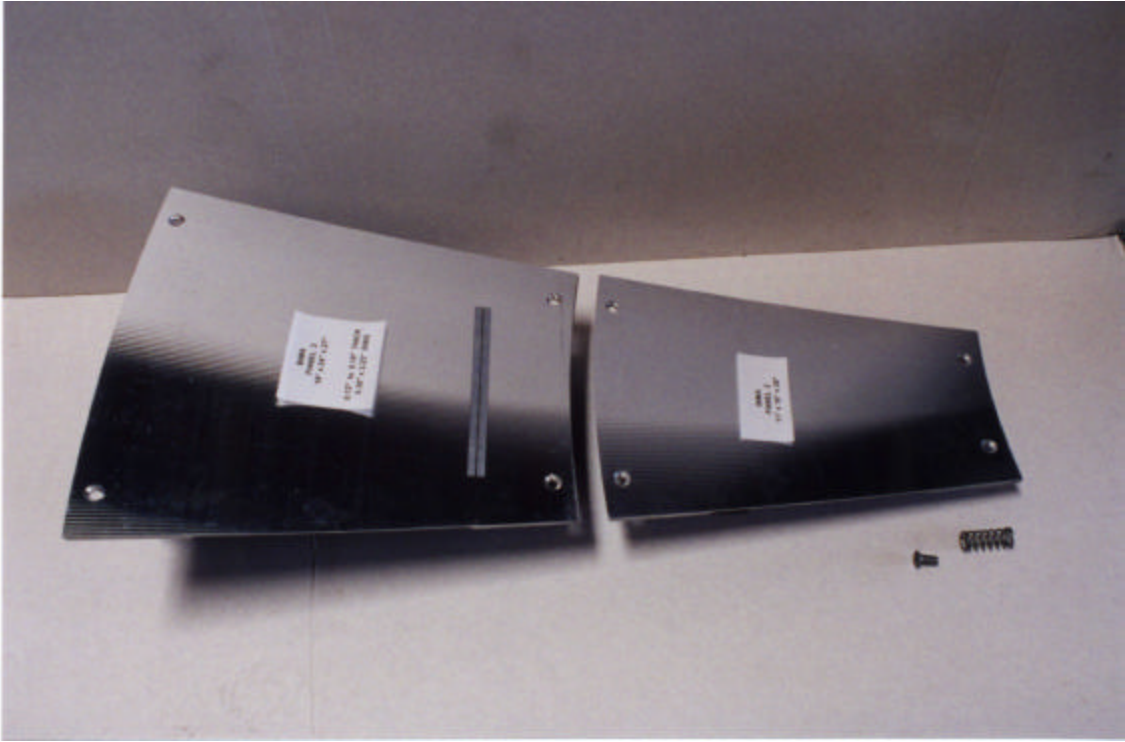


Figure 3.2.2-1. Front side of BIMA aluminum panels.

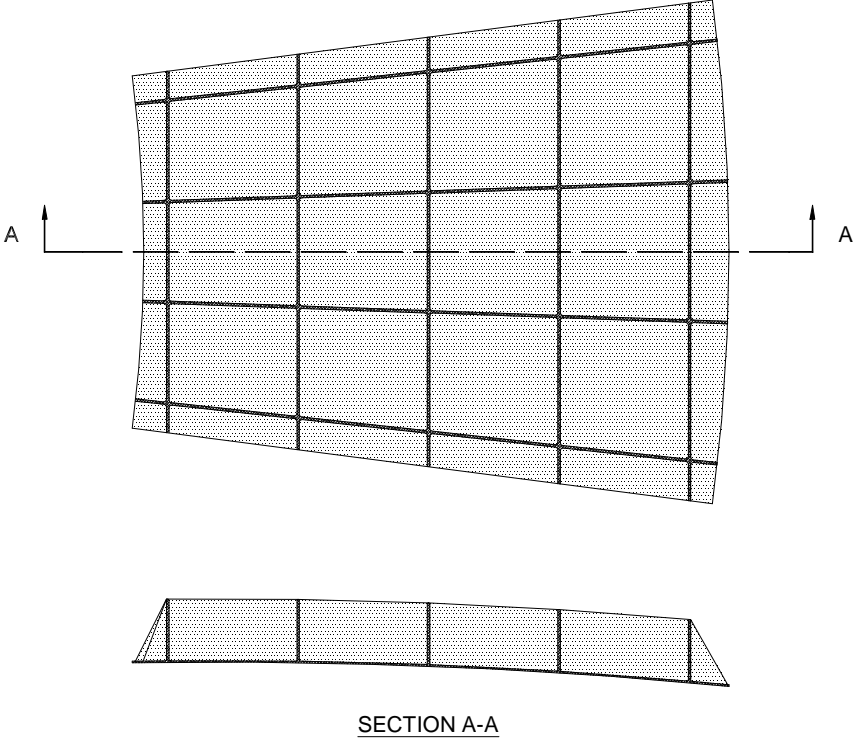


Figure 3.2.2-2. Proposed antenna panel.

3.2.3 APEX STRUCTURE

The apex structure and quadripod provide a stable support for the secondary mirror and stiffen the BUS, particularly against astigmatic deformation. The secondary mirror drive has three translation axes for focus and optical alignment. For modeling purposes, a mass of 50 kg was assumed for the drive mechanisms. The quadripod legs are high modulus CFRP (207 GPa) to minimize their required cross section. The legs pass as far outboard of the secondary mirror as possible and mount close to the edge of the primary to minimize blockage.

3.2.4 RECEIVER CABIN

The receiver cabin is designed to accommodate equipment such as the receiver package, electronic racks, and optical devices in front of the receiver. In this design, the cabin also acts as a supporting structure for the CFRP dish structure. The cabin side plates and stiffening beams are supported by the elevation axles through a roller bearing on each side. Front and back plates join the side plates and they form a 3-m by 3-m box with a height of 2.7 m. The counterweight volume is located under the floor plate of the cabin as shown in Appendix A-4. The top plate of the box has a large hole to provide access to the part of the cabin volume within the hub of the BUS. Because the cabin has structural plates on all six sides, it is very rigid; from each of the four top corners five plates spread out to support sixteen points equally spaced around a circle whose radius is that of the base of the BUS. The stiffness of the support plates is optimized to deflect equally when supporting the weight of the dish at zenith. These support plates are shown in Figure 3.2.4-1, where the top ring plate is

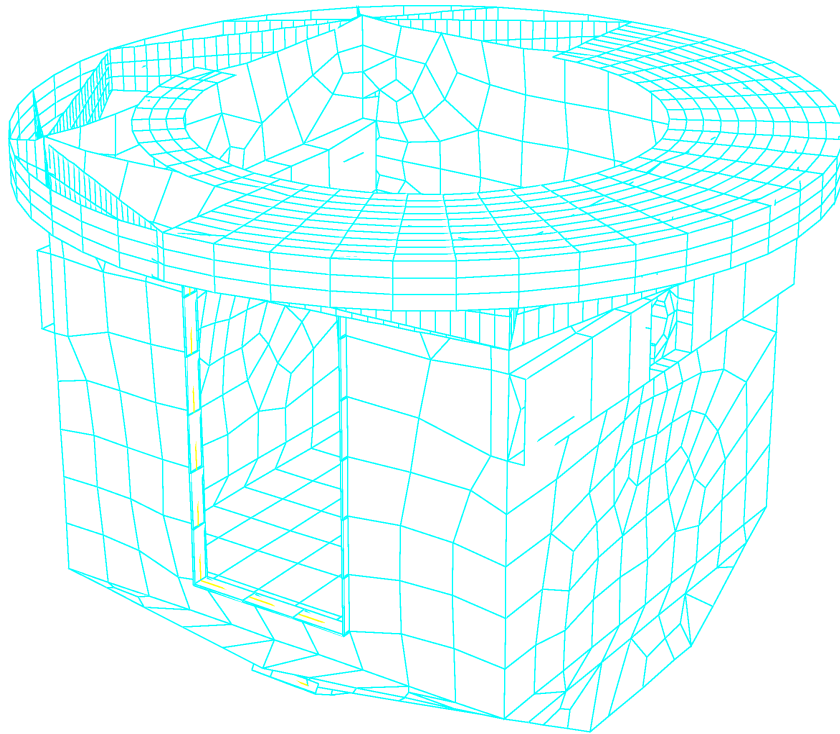


Figure 3.2.4-1. Antenna receiver cabin structure.

partly removed. Radially soft flexures connect the receiver cabin to the BUS to accommodate differential thermal expansion.

To access the cabin space, a door 1 m wide by 2 m high is provided on the front side. Around the door, beam members are used for local stiffening purposes. The elevation drive ring is attached to the cabin back and counterweight volume. Very little counterweight is required; the cabin structure nearly balances the dish. The receiver center of mass is very close to the elevation axis so that the dish is adequately balanced with or without the receiver installed. A remote-controlled shutter covers the receiver cabin membrane window in bad weather.

3.2.5 YOKE

The yoke is fabricated from welded steel plate. It is the largest and, in some ways, the most critical part of the mount. Because of its location near the top of the mount, both its mass and stiffness are important factors in determining the lowest natural modes of the telescope which are important for the dynamic performance. Its stiffness-to-mass ratio has been roughly optimized, but further optimization could increase the stiffness-to-weight ratio by 10 to 20 percent..

An unconventional feature of the yoke design is that the elevation axles are attached to the top of the yoke arms and the elevation bearings are flange-mounted in the walls of the cabin. In this way the elevation bearings apply a negligible bending load to the cabin structure. Instead, the bending load is applied to the top of the yoke arms, which handle it more easily than the cabin structure would. Furthermore, the bending load is independent of the cabin elevation angle.

The geometry of the internal structure of the yoke has been designed with ease of fabrication as a consideration, so that the yoke has no inaccessible cavities or welds.

Because the large diameter, thin-section azimuth bearing is not intrinsically stiff, both the yoke and the base are carefully designed to provide uniform loading of the bearing. The weight of the yoke, and the elevation structure it carries, is uniformly distributed about the circumference of the bearing. Likewise, the base supports the bearing with uniform stiffness about its circumference. With this arrangement, the bearing remains planar regardless of the azimuth angle of the telescope. This helps reduce the turning friction of the bearing and greatly reduces the wobbling of the azimuth axis direction with changes in azimuth angle. Failure to optimize the stiffness of the bearing mounting faces on the yoke and base would cause the bearing to be distorted by the weight of the telescope no matter how flat the unloaded mounting faces had been machined.

Within each arm of the yoke is a CFRP “reference structure” which is a major part of the metrology system, and is discussed further in section 4.1. Each reference structure is attached to the yoke structure near the azimuth bearing and extends upward to provide attachment for the elevation encoder and reference points for measuring yoke deflection.

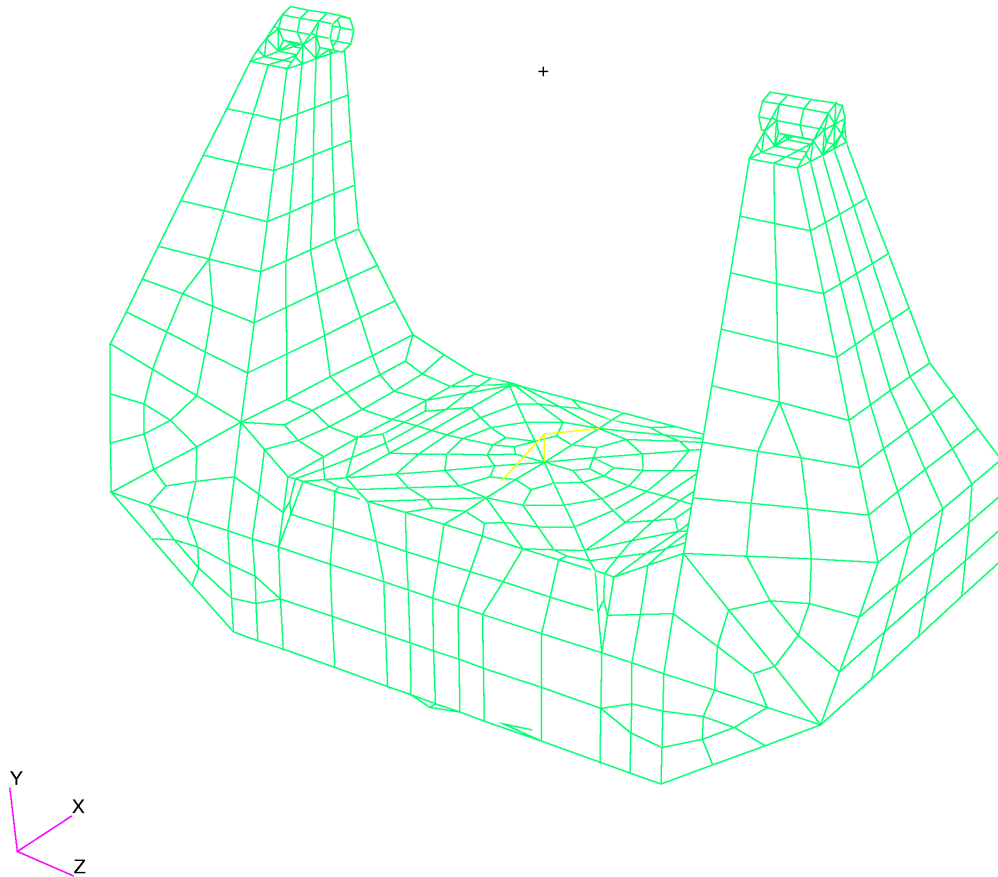


Figure 3.2.5-1. Antenna yoke structure.

3.2.6 BASE

As stated in the previous section, an important feature of the base design is that it provides uniform support for the azimuth bearing to maintain bearing flatness. The vertical stiffness of 12 equally spaced points about the azimuth bearing perimeter has been optimized so that their vertical deflection is equal to within 0.5 microns when equally loaded.

The antenna base interfaces to the foundation at only 3 points to provide a kinematic support of the antenna as shown in Figure 3.2.6-1. The height of the interface pads on each base is adjustable, as is the height of each pad on the foundation, as shown in Figure 3.2.6-2. With this scheme, every antenna and foundation can be pre-leveled, so when an antenna is moved to a new foundation, it will be adequately level without any special adjustment. This will allow the rapid relocation of antennas, which is desirable. Choosing a 3-point kinematic interface, rather than some over-constrained geometry, also helps to maintain a flat azimuth bearing. By designing one leg's interface to locate in two horizontal dimensions, a second leg's interface to locate in one horizontal dimension, and the third leg to locate only vertically, the antenna azimuth angle is predetermined as well. Each of the three legs of the base is bolted to the foundation with a single Acme threaded screw.

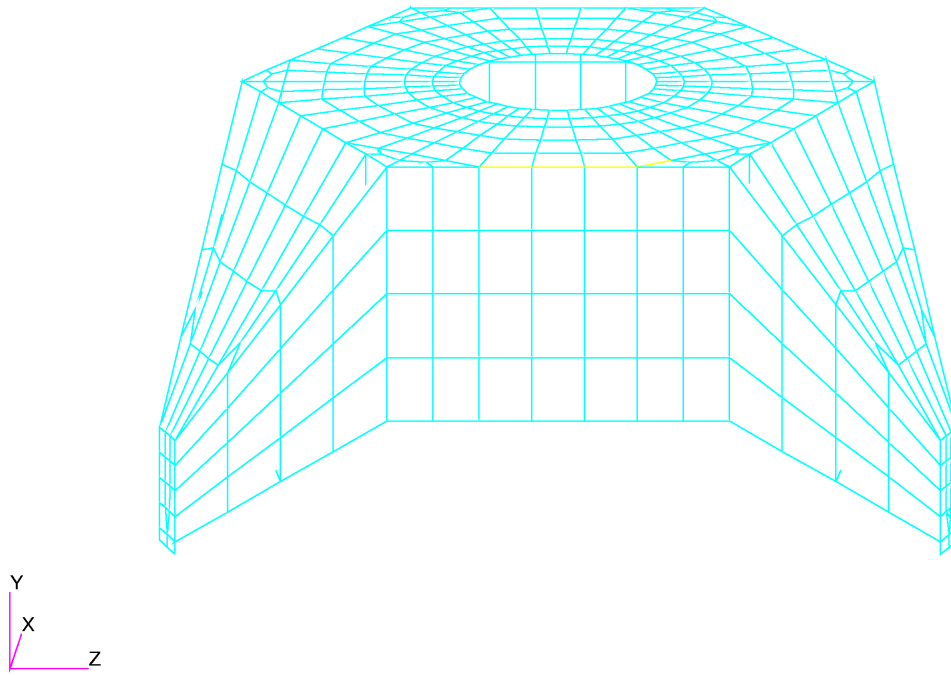


Figure 3.2.6-1. Antenna base structure.

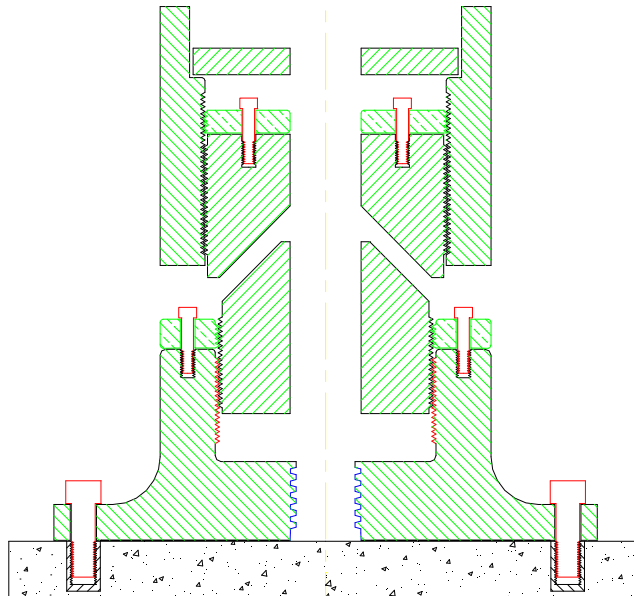


Figure 3.2.6-2. Antenna base to foundation connection - leveling joint.

3.2.7 BEARINGS

The azimuth bearing is either a two-row angular-contact ball bearing or possibly a crossed-roller bearing [10]. The roller path is about 2.4 meters in diameter. Both of these bearing types have a very high stiffness-to-turning friction ratio and are less costly than the three-row-roller bearing, which also has excellent stiffness-to-turning friction performance. Besides its higher cost, the other disadvantage of the three-row-roller bearing is that it is not usually made with a preload in the radial direction. The two-row angular-contact bearing or the crossed-roller bearing would probably be preloaded to approximately $10E11$ in-lb/rad overturning stiffness.

The elevation bearings are spherical roller bearings. The bearings on both yoke arms are designed to carry thrust loads. Because the walls of the receiver cabin and the yoke arms are somewhat compliant, the bearings can easily carry any opposing thrust loads which might result from temperature differences or loads applied during assembly.

3.2.8 DRIVES

Similar friction drive units are planned for the elevation and azimuth drives. An example is shown in Figure 3.2.8-1 [10]. Each consists of a small diameter roller with a torque motor mounted directly on one end and a gear box and electric brake mounted on the other end. The roller runs against the elevation or azimuth drive ring of the telescope (the azimuth ring may actually be the inside or outside ring of the azimuth bearing). By using a gearbox to drive the brake, the required size of brake is greatly reduced; a planetary gearbox is chosen because it can be back driven even with a fairly high gear ratio, say 100:1.

The drive roller is pressed against the drive ring by a pair of idler wheels. To increase the stiffness of the drives, a carbide roller shaft may be desired. Hard coatings, often used on cutting tools, such as TiN, may be useful to reduce the likelihood of welding between the drive roller and the driven wheel. The drive roller is constrained axially to the yoke - it is not in a separate carriage which can float axially to track the drive ring. Instead, the drive roller axis must be very carefully aligned with the antenna axis to avoid excessive thrust loading. The antenna structure must accommodate the thrust loads that will be generated without degrading pointing in a nonrepeatable way.

A single drive unit is probably adequate for the elevation axis; two or three identical units may be used for the azimuth axis.

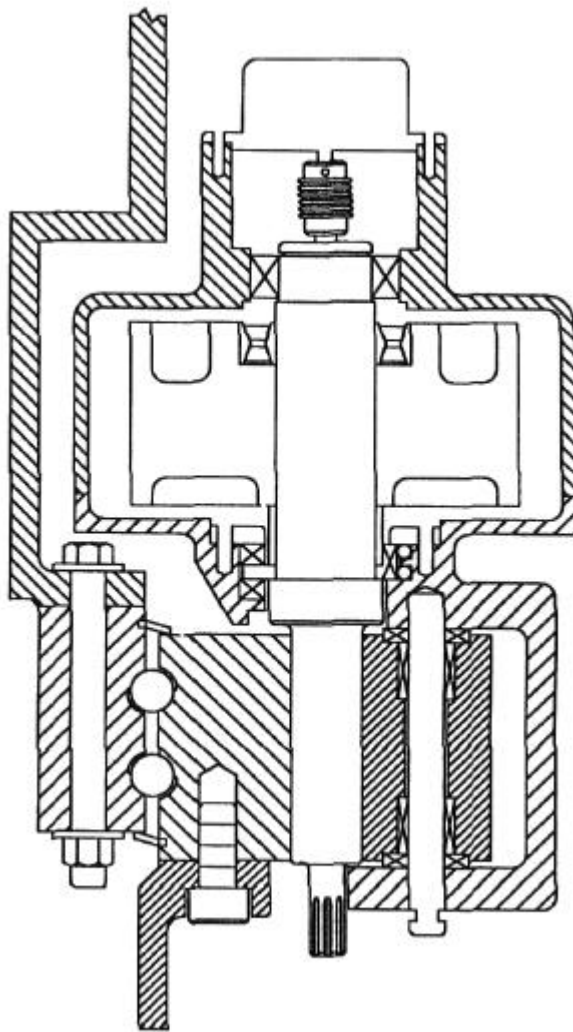


Figure 3.2.8-1. Azimuth friction drive assembly cross section.

3.2.9 CABLE WRAP

The azimuth cable wrap employs igus® Energy Chain [11] as a flexible cable carrier in a rotary fashion as shown in Figure 3.2.9-1. A particular model suited for this application is the 5050 series. The Energy Chain will allow us to rotate 540 degrees and have the cables cleanly packaged without kinking or chafing. Cables can also be segregated by size or type in this system by using separators on the interior of the Energy Chain.

The cables will enter the antenna base through a bulkhead fitting on the base of the antenna. Cables are then carried into the Energy Chain inside the antenna base. The stationary end of the chain is mounted to the inside diameter of the base. The rotating end is mounted to a 1150 mm (45.3 inch) diameter drum that rotates with the yoke. The cables exit the Energy Chain and enter another cable carrier that leads into the base of the yoke.

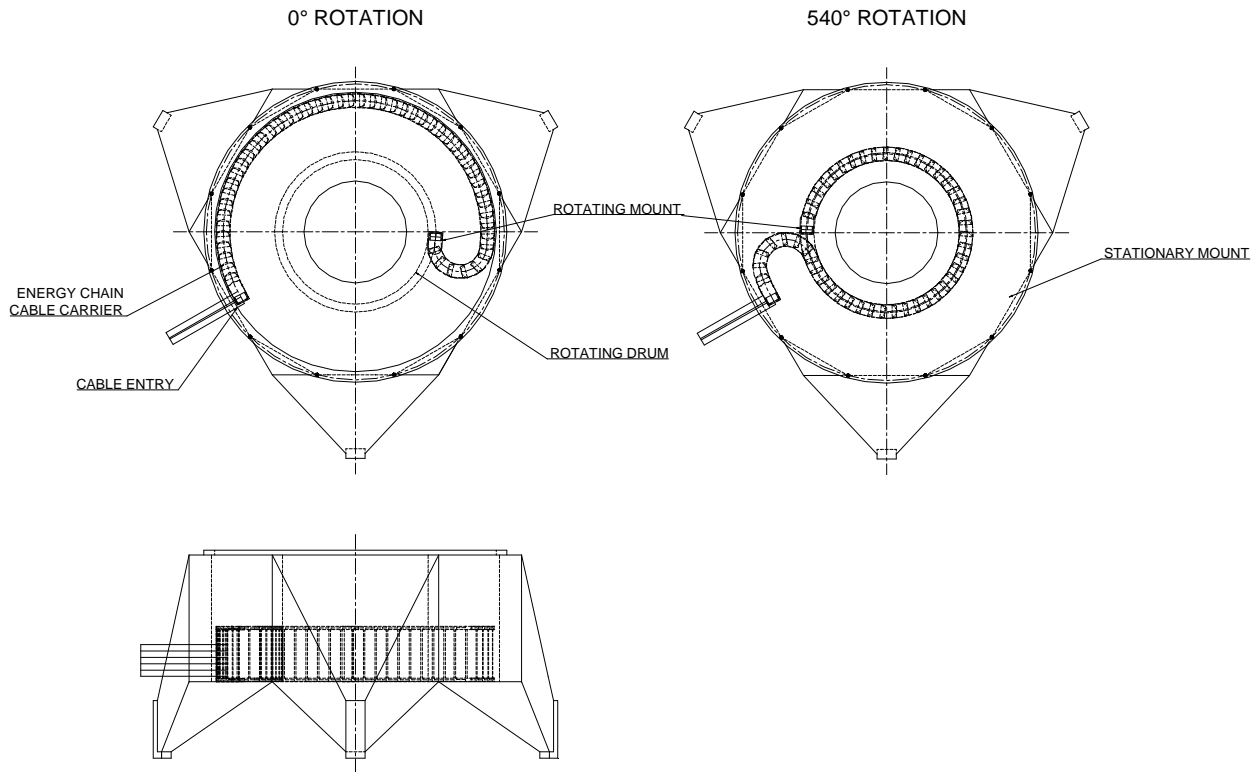


Figure 3.2.9-1. Azimuth cable wrap.

3.2.10 THERMAL CONTROL

The receiver cabin temperature is regulated to provide a controlled environment for the receiver and any electronics which reside there. In this design, it may be preferable to place the insulation on the outside of the receiver cabin walls, the advantage being that the cabin walls are available to mount equipment and that the cabin dimensions will change far less than if the cabin structure tracked the diurnal temperature swing. The cabin walls and yoke arms are compliant enough to accommodate the swelling of the yoke as it tracks changes in the ambient temperature.

Several other parts of the telescope may benefit from some thermal control. Sunshades which protect the steel structure from direct sunlight can be used to lengthen the time constants for thermal distortion of the antenna structure. While the antenna metrology system can measure and correct most of the thermal distortion, a slower thermal variation is easier to correct. Sunshades are proposed for covering the sides and rear of the BUS, mainly for snow, ice, and UV protection.

3.3 FOUNDATION

Each antenna will be moved between several observing stations. There will be about thirty-six antennas with about 180 observing stations.

At this time little information on soil properties is known. However, it is expected that the soil is loose volcanic material with a modulus of elasticity similar to what is found on Mauna Kea, Hawaii, of about 100 MPa. The foundation will have a large contact surface to spread the load and produce a stiff support.

A conceptual foundation design is shown in Figure 3.3-2. The top surface of the foundation is just above grade to permit the transport to cross the foundation. This will be particularly important for the compact array. The antenna foundation interface fittings can be covered to protect them and the transporter tires from damage during transporter crossings.

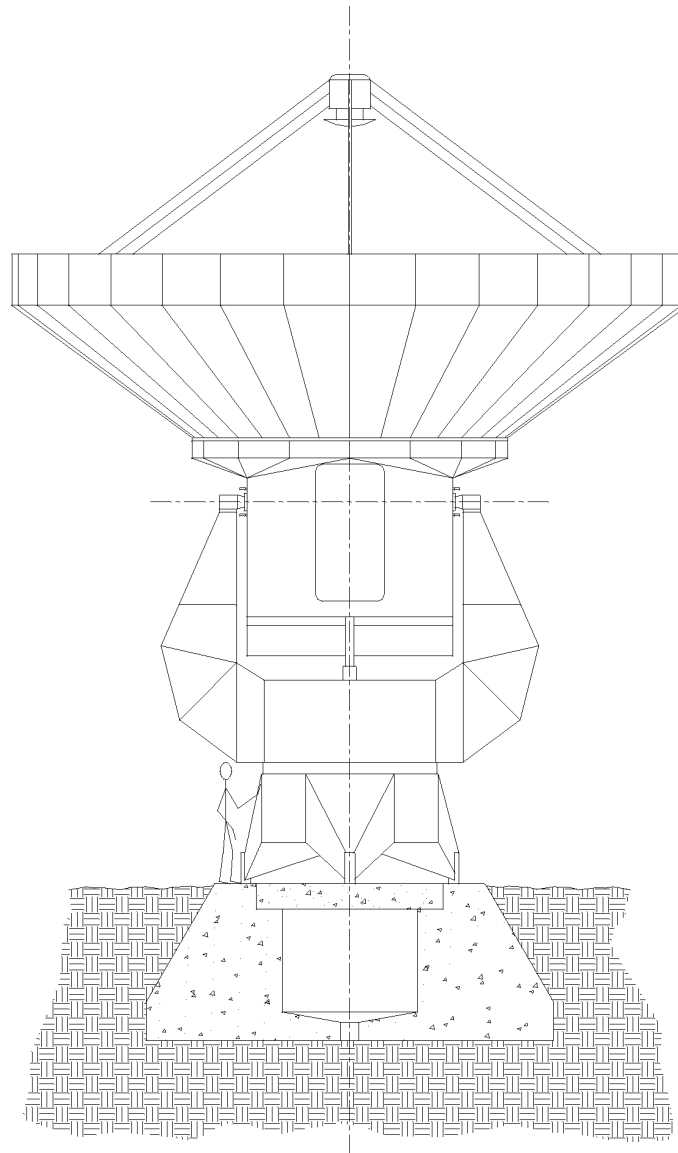


Figure 3.3-2. Antenna foundation.

3.4 CONTROL SYSTEM

The conceptual control system design is outlined in the drawing in Appendix C. For this design, each antenna has its own control system. The antenna will be commanded from a central control computer. Each antenna will receive commands through a communications fiber link and timing bus.

The main servos are thought to have cascade controllers with current, velocity, and position loops. The velocity signals are generated from the encoder readings. Brakes on the main axes will be operated automatically. The main axes will also have over-speed protection.

Corrections from the metrology system are fed into the Antenna Control Unit (ACU) and compensations are made in the control system to correct for pointing errors.

4. ANTENNA METROLOGY

In order to achieve the desired pointing accuracy and phase stability, this design uses additional encoders beyond the usual elevation and azimuth axis encoders. The major additional elements consist of a "reference structure" to measure the deflection of the yoke and tiltmeters to measure the tilt of the antenna base and foundation [12]. As it currently stands, the design contains no additional measuring elements above the elevation axis. However, it was recently discovered that deflections above the elevation axis may be only marginally acceptable; optimization of the cabin and dish structure or adding metrology elements between the dish and elevation encoder may be required.

The reference structure in the yoke arms and the tiltmeters near the azimuth bearing are not required or expected to remove all pointing or delay errors with 100 percent accuracy. Rather, by aiming to remove only 90% or 95% of the error due to deflection of the mount and foundation, the design can be very conservative and assured of success; the reference structure has no moving or massive parts supported by the encoder bearings.

4.1 INDEPENDENT REFERENCE ARMS

The main element of the metrology system is a CFRP reference structure within each arm of the yoke. This structure carries no load, but simply provides points near the top of the yoke arms and elevation encoder, which are accurately referenced to the structure just above the azimuth bearing. A pair of displacement sensors in each yoke arm measure the vertical and horizontal deflections of the yoke arms due to thermal and/or wind loads. The four sensors allow measurement of tilt, twist, and translation of the elevation axis relative to the plane of the azimuth bearing and the azimuth axis encoder. They allow removal of azimuth pointing errors and geometric delay change due to yoke deflection. Many displacement sensors have ample sensitivity, stability, and range; one possible choice would be the Schaevitz model 050HR LVDT. The elevation encoder is also attached to the top of one of the reference arms, which automatically removes elevation pointing error due to yoke deflection. The reference structure is constructed from CFRP and has very small coefficient of thermal expansion (on the order 1 ppm/C) and resonant frequency (on the order of 50 Hz) much higher than the dominant low frequency modes which affect servo performance.

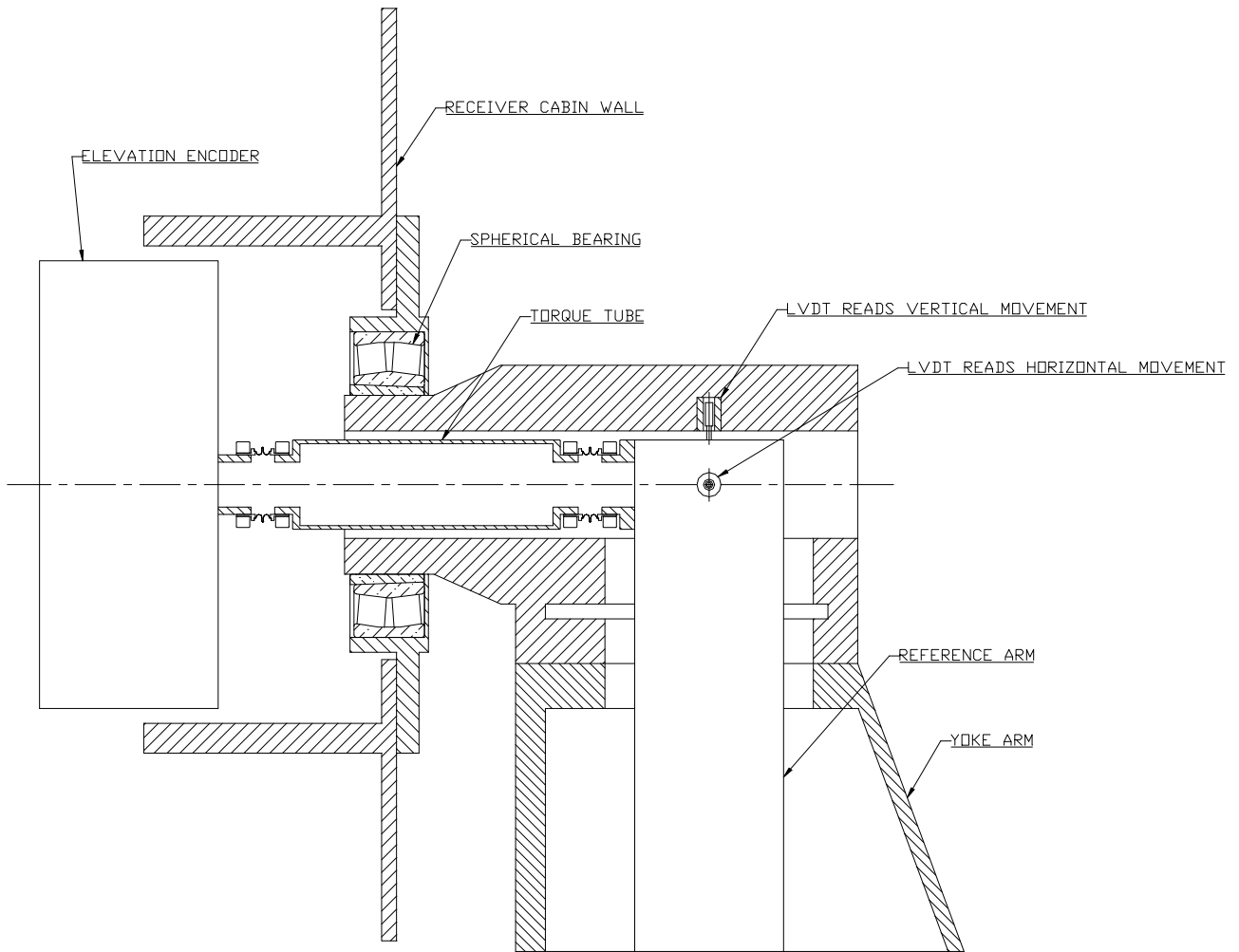


Figure 4.1-1. Independent reference arm coupling to encoder.

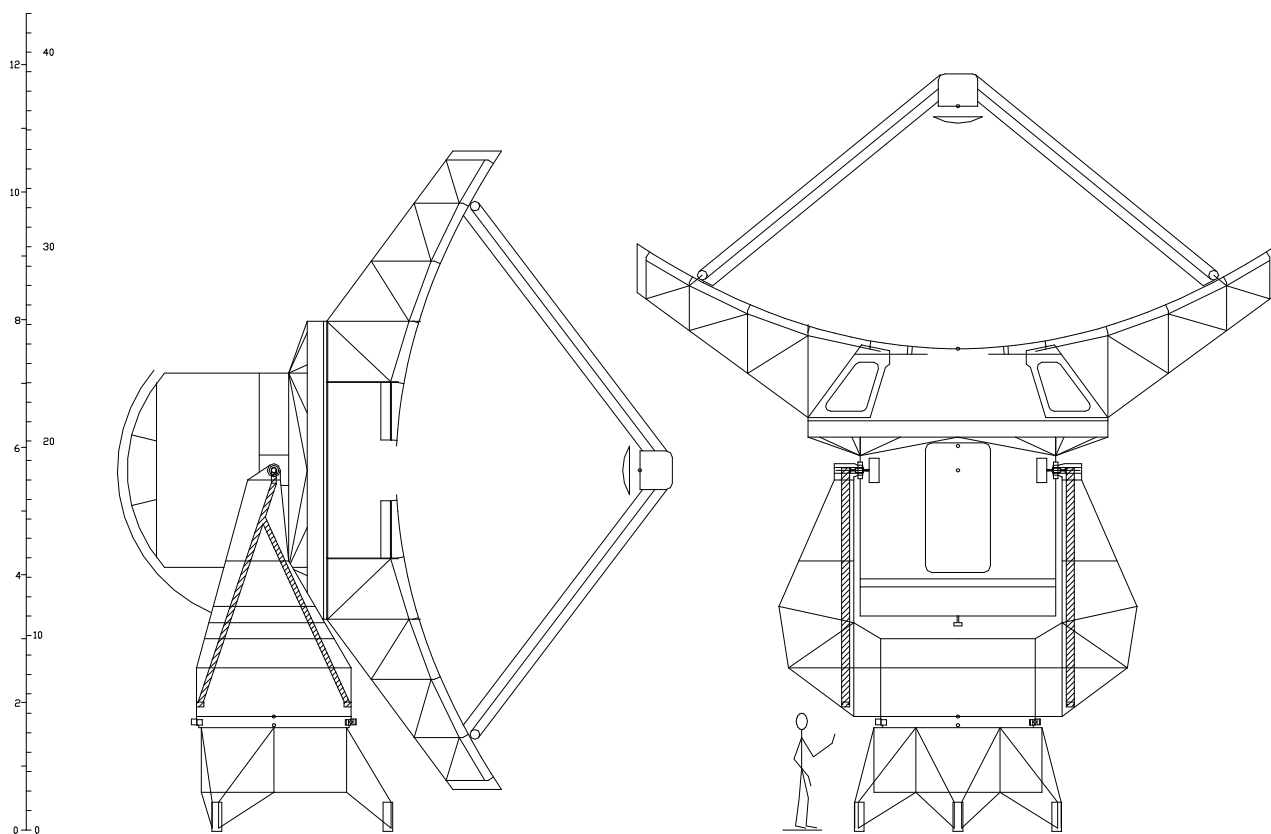


Figure 4.1-2. Independent reference arms.

4.2 TILTMETERS

Fixed, 2-axis tiltmeters are placed on the top of the antenna base, just below the azimuth bearing. A similar single axis tiltmeter is placed in the bottom part of the yoke, near the azimuth axis.

The tiltmeters which are located at the top of the antenna base are used to measure the tilt of the azimuth bearing. This tilt may have slowly varying components due to an antenna being imperfectly leveled or the settling or shift of an antenna foundation. The tilt may also have more rapidly varying components due to uneven solar heating of the antenna base or wind loading of the antenna structure. These tiltmeters are relatively free from acceleration during antenna movement and should give reliable readings except for the possibility of instrumental drift. Instrumental drift is to be removed by periodic comparison to the rotating tiltmeter.

The tiltmeter which rotates with the yoke can be continuously read while the antenna is steadily rotated in azimuth in order to determine the orientation of the azimuth axis and to measure wobble of the axis as a function of azimuth angle. Because it rotates with the yoke, any DC drifts of this tiltmeter or its mount are of no consequence. However, this tiltmeter is not likely to be located sufficiently close to the azimuth axis to give readings accurate to the 0.1 arcsec level while the antenna is accelerating in azimuth.

Thus, the rotating and the fixed tiltmeters are both necessary to achieve the total performance necessary. One possible choice for the tiltmeters is the Applied Geophysics model number 520 which is in use at the Owens Valley Radio Observatory [13][16].

4.3 OPTICAL POINTING TELESCOPE

The optical pointing telescope is designed to improve pointing of the telescope. This device will be mounted on the telescope BUS at a location where motion is representative of the radio beam. By using the pointing telescope to point at several hundred stars at night, the mount of the telescope can be characterized very well to improve the pointing model of the telescope. This pointing telescope will also be used to test the pointing and servo performance of the antenna.

4.4 TEMPERATURE PROBES

The antenna has temperature probes to monitor the temperature of the antenna structure; it may be possible to correlate temperature effects with pointing errors [14] [15]. Initially, these probes will be used to identify undesirable thermal gradients. If correlations are found, they could be used for pointing corrections.

5. ANTENNA PERFORMANCE

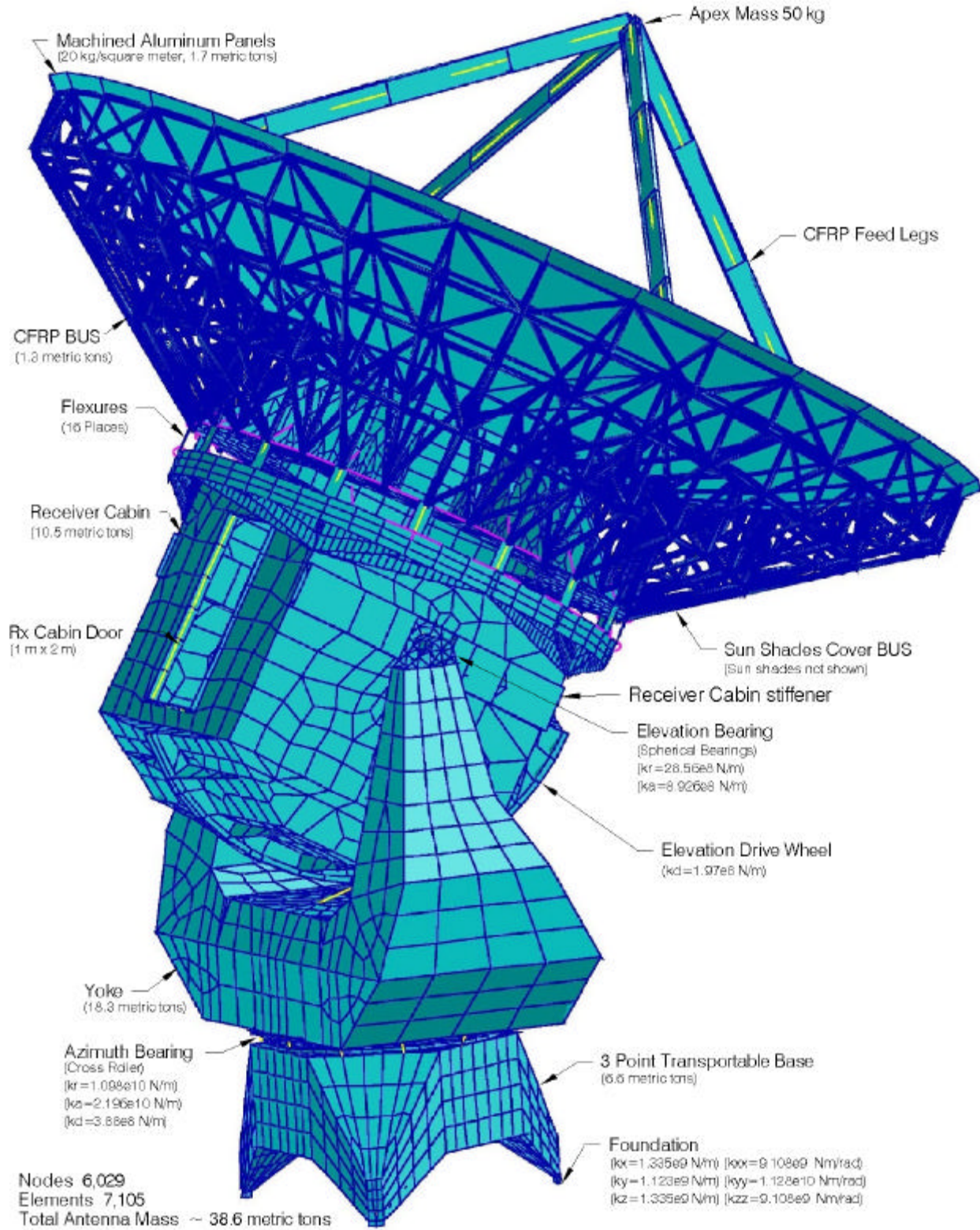


Figure 5.1-1. FEA model of 10-meter antenna design.

5.1 SURFACE ERROR BUDGET

The surface error budget is listed in Figure 5.1-1.

<u>SURFACE ERROR BUDGET</u>	
BACKING STRUCTURE (<i>Uni-axial CFRP</i>)	
Gravity	8.7 μm
Wind (13 m/s)	3.0 μm
Absolute temperature ($ \Delta T < 25\text{ C}$)	1.0 μm
Temperature gradients	3.0 μm
	Total (rss) = 9.7 μm
PANEL (<i>Aluminum</i>)	
Manufacturing, ageing, scattering	6.0 μm
Gravity	1.5 μm
Wind (13 m/s)	0.5 μm
Absolute temperature ($ \Delta T < 25\text{ C}$)	2.0 μm
Temperature gradients	2.0 μm
	Total (rss) = 6.8 μm
SECONDARY MIRROR (<i>Aluminum</i>)	
Manufacturing, ageing, scattering	5.0 μm
Gravity	1.0 μm
Wind (13 m/s)	0.5 μm
Absolute temperature, Temp. gradients	3.0 μm
Alignment	3.0 μm
	Total (rss) = 6.6 μm
PANEL MOUNTING	
Temperature difference 4 C panel-panel	2.0 μm
Panel location	0.5 μm
	Total (rss) = 2.1 μm
HOLOGRAPHY	
Measurement and adjustment	10 μm
	Total (rss) = 10 μm
TOTAL (rss)	17 μm

Figure 5.1-1. Surface error budget.

5.2 OPTOMECHANICAL PERFORMANCE

5.2.1 FEA MODEL DESCRIPTION AND STRUCTURAL ANALYSIS

Finite element models of the antenna were constructed using MSC/PATRAN software [17]. Individual models were used for static and dynamic structural analyses. The structural analysis was performed by using MSC/NASTRAN software [18].

In general, each three-dimensional model consists of beam and plate elements to represent the overall antenna mass and stiffness. Scalar spring elements are used to model discrete stiffness for items such as joints, bearings, and foundation. Lumped mass elements are used to represent concentrated nonstructural mass.

In the static structure model, the surface panels were modeled as plate elements of the same weight, but with negligible stiffness. By doing so, the surface deformations could be expressed and the wind pressure could be applied. For dynamic analysis, the panels were modeled as concentrated masses.

The various parts of the antenna are constructed of either steel, aluminum, or carbon fiber reinforced CFRP materials. The properties used to represent these materials are summarized in Table 5.2.1-1.

Materials	Modulus GPa	Poisson ratio	Density kg/m ³
Steel	200	0.27	7800
Model panel	0.37E-9*	0.33	2800
CFRP beam	124	0.3	1600
Feedleg CFRP	207	0.3	1600
CFRP plate	62	0.3	1600

*Simulated property to model panels.

Table 5.2.1-1 Material properties.

In the modeling process, isotropic material properties were assumed even for CFRP beam or plate members. The joints of CFRP structures are not modeled in detail. The model involves many inclined plate elements. To suppress grid point singularities, a larger K6ROT value is used in the analysis for some cases in the NASTRAN run.

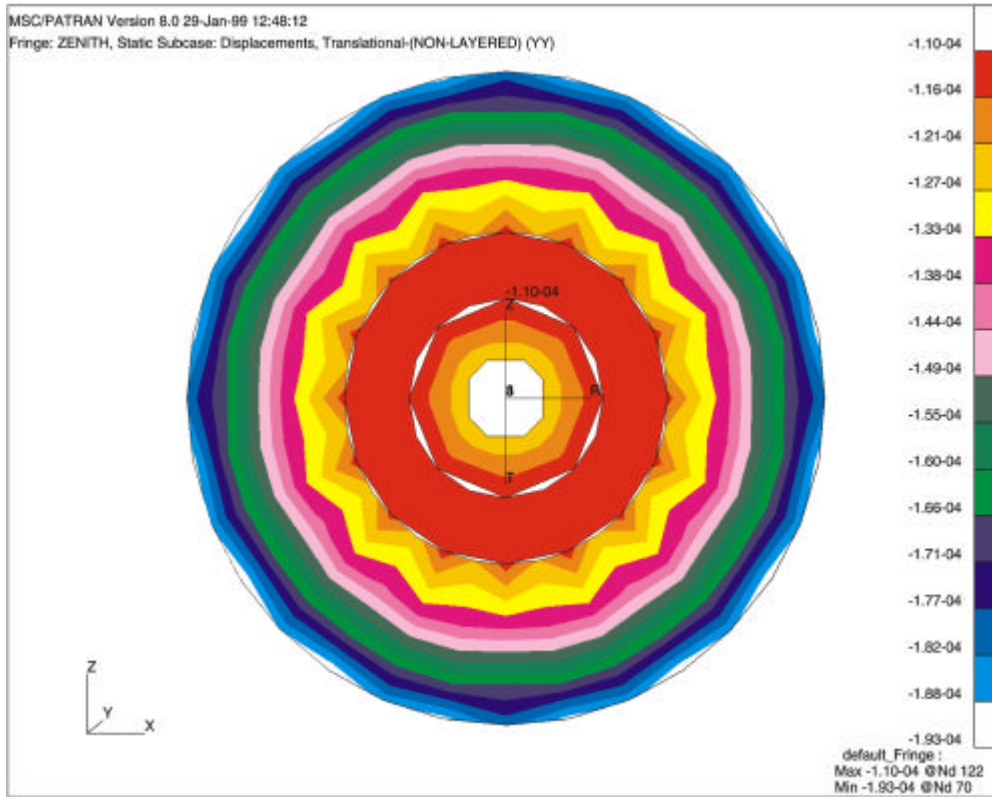
The present antenna models are separated into five parts: dish, cabin, yoke, base, and foundation. In total it has 6,029 nodes and 7,105 elements. The y-axis is upward and the z-axis is parallel to the elevation axis.

5.2.2 GRAVITY LOAD

Gravitational deflection of the BUS is one of the major contributors to the total surface error. The philosophy chosen for setting the primary mirror surface is to minimize the maximum surface error over the zero-to-90 degree elevation range. Since the dish structure has a linear response to gravitational loading, the load condition for which the dish should be perfect lies mid-way between the extreme loading conditions which occur at 0 degrees elevation and 90 degrees elevation; this load condition is 0.5 g in the direction opposite to the bore sight, and 0.5 g perpendicular to that direction (in the plane perpendicular to the elevation axis). For this dish design, the surface error as a function of elevation is as shown in Figure 5.2.2-3. Because of the fourfold rotational symmetry of the BUS, the response to gravitational loading in the direction of the bore sight is symmetric; the response to loading in the perpendicular direction is antisymmetric; and knowing the response to the loading in these two directions is sufficient to calculate the response to loading in any direction (the bore sight direction and the direction perpendicular to that are the principle directions - the cross term is zero).

For the current state of optimization, the surface error due to a 1 g change in the axial loading is 7.6 microns RMS, and the error due to a 1 g change in lateral loading is 15.6 microns RMS deviation from the best fit paraboloid. Figures 5.2.2-1 and 5.2.2-2 show the surface deviation before removing the best fit paraboloid. With the mini-max optimization, the maximum gravitational surface error is less than 8.7 microns over the zero-to-90 degree elevation range. The gravitational surface RMS is less than 5 microns over more than 80% of the sky above 30 degrees elevation. Note that for this choice of surface optimization, the dish surface is not perfect for any elevation angle.

The gravity load also produces changes in antenna pointing and path length. Pointing changes are typically absorbed into two terms of the elevation pointing equation. Path length changes are repeatable and similar from one antenna to another.



Figur5.2.2-1. Response to 1 g gravity load at zenith.

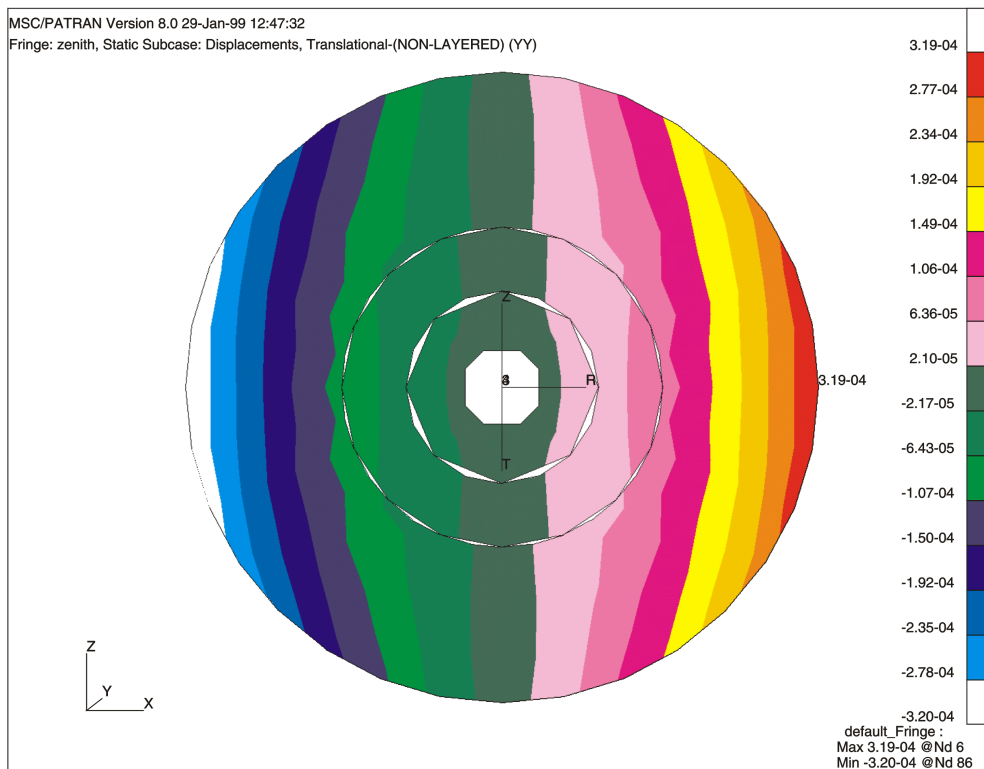


Figure 5.2.2-2. Response to 1 g gravity load at horizon.

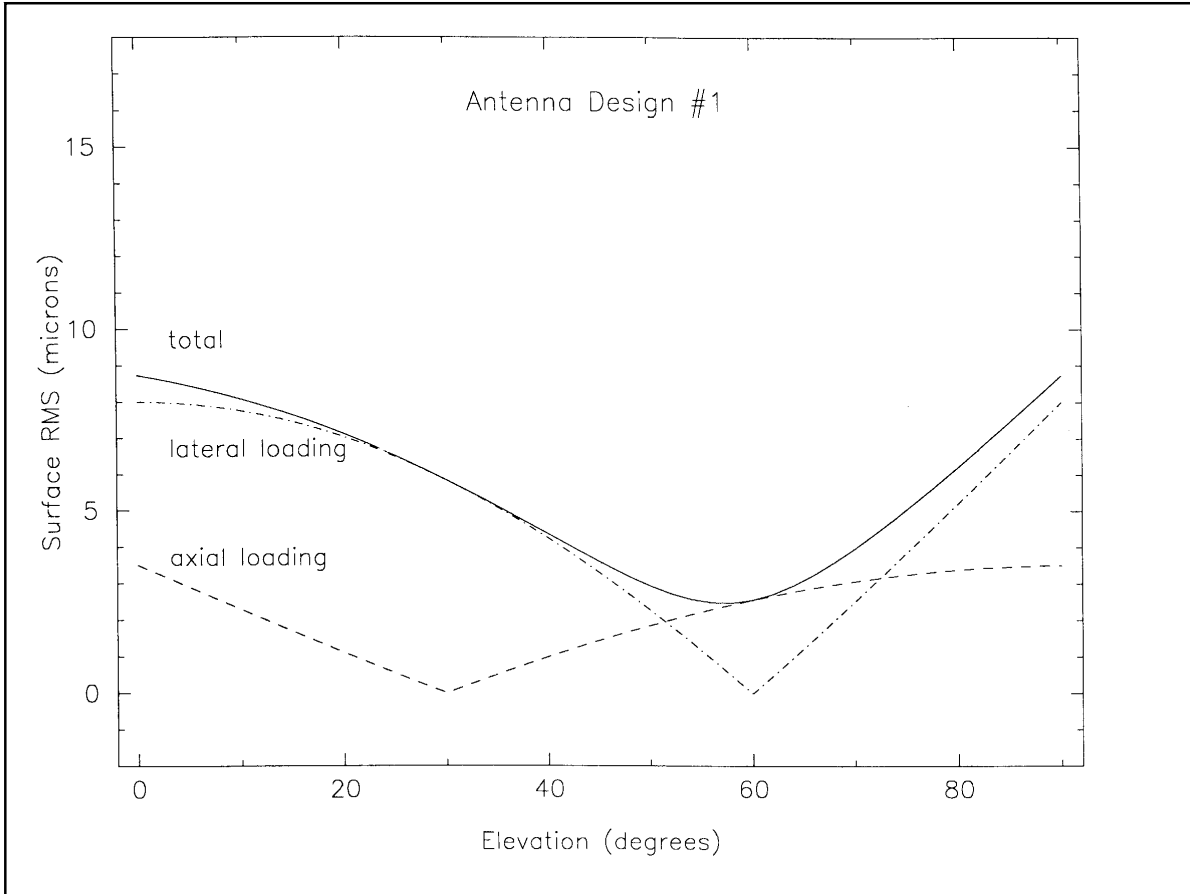


Figure 5.2.2-3. Elevation surface RMS optimization.

5.2.3 WIND LOAD

The purpose of the wind load analysis is to determine pointing errors and check stress levels. The operational wind condition is used in the pointing error case, and the maximum wind velocity is used in the stress level case. The wind loads on a structure are a function of wind velocity. Because the wind speed varies with time, the wind analysis should consist of calculating the response to a number of representative wind spectra. However, at this time we have analyzed only the response to a steady wind.

We have calculated the pointing change for zenith pointing (wind perpendicular to elevation axis) and for horizon pointing (dish facing directly into the wind). In the analysis, we have applied the wind loadings to the dish surface, feedleg surfaces, and secondary mirror unit. Wind loadings on other parts of the antenna are not included. The dish surface wind loading distributions for the zenith and horizon pointing are from Levy and Fox [19] [20] [21].

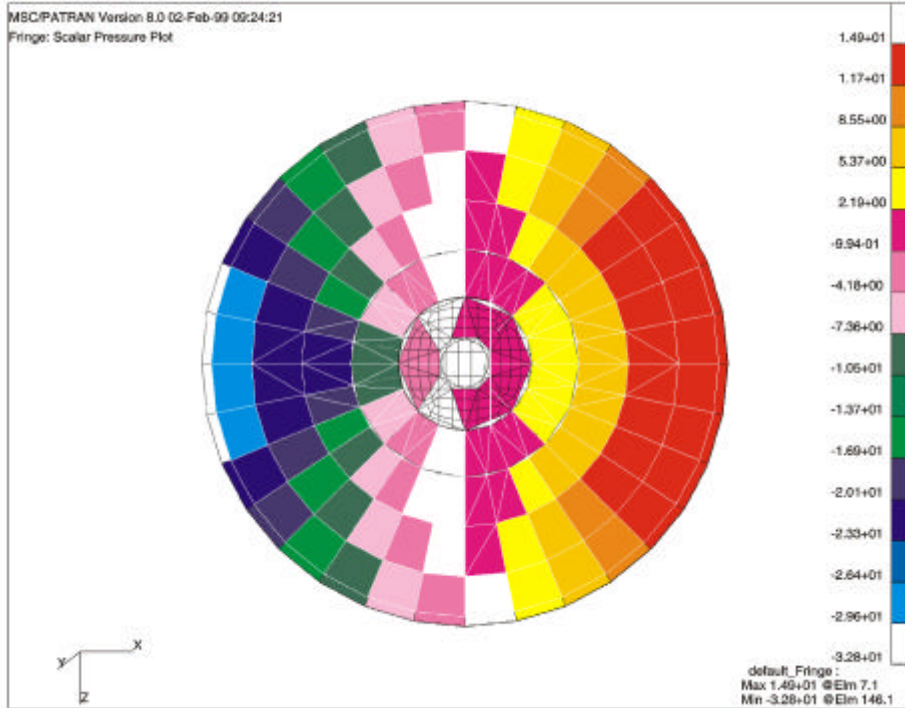


Figure 5.2.3-1. Zenith wind loading.

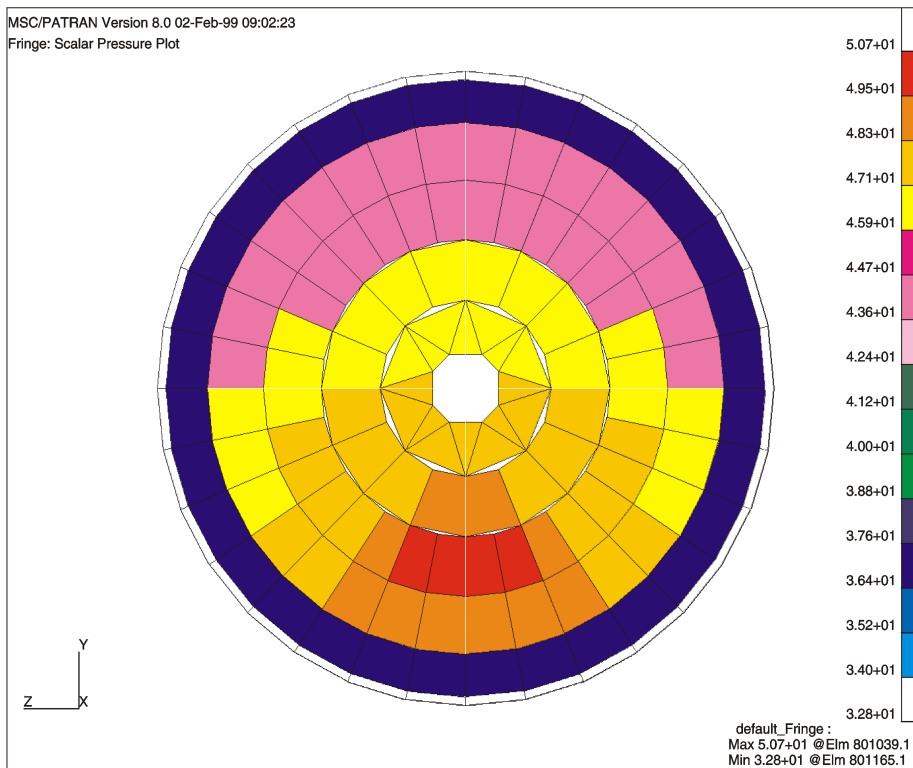


Figure 5.2.3-2. Horizon wind loading.

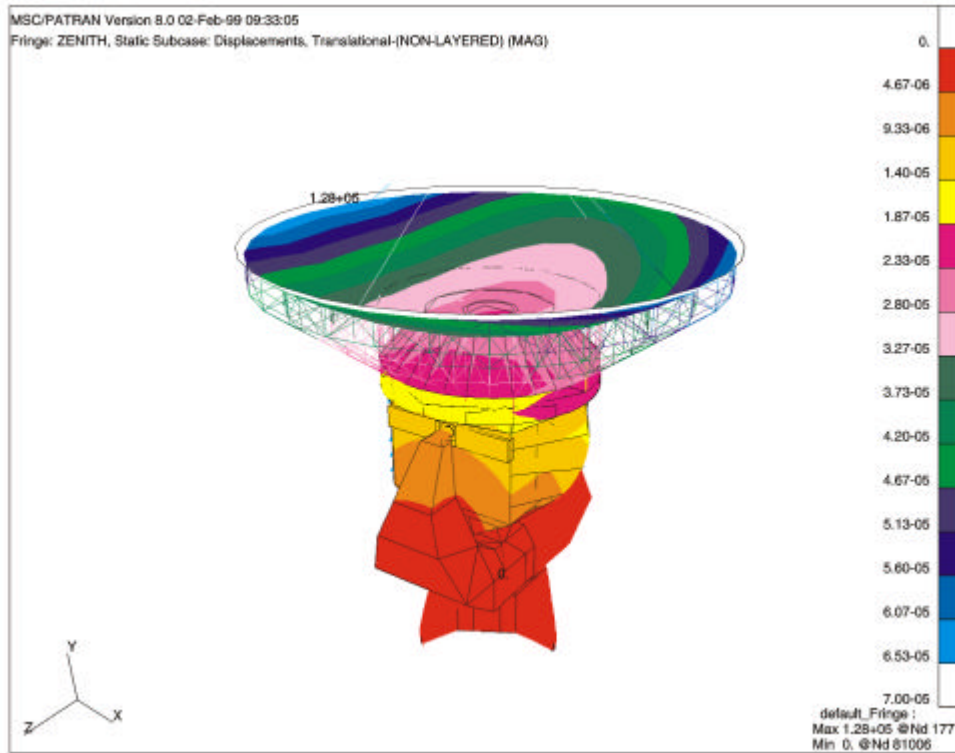


Figure 5.2.3-3. Zenith wind pointing deflection.

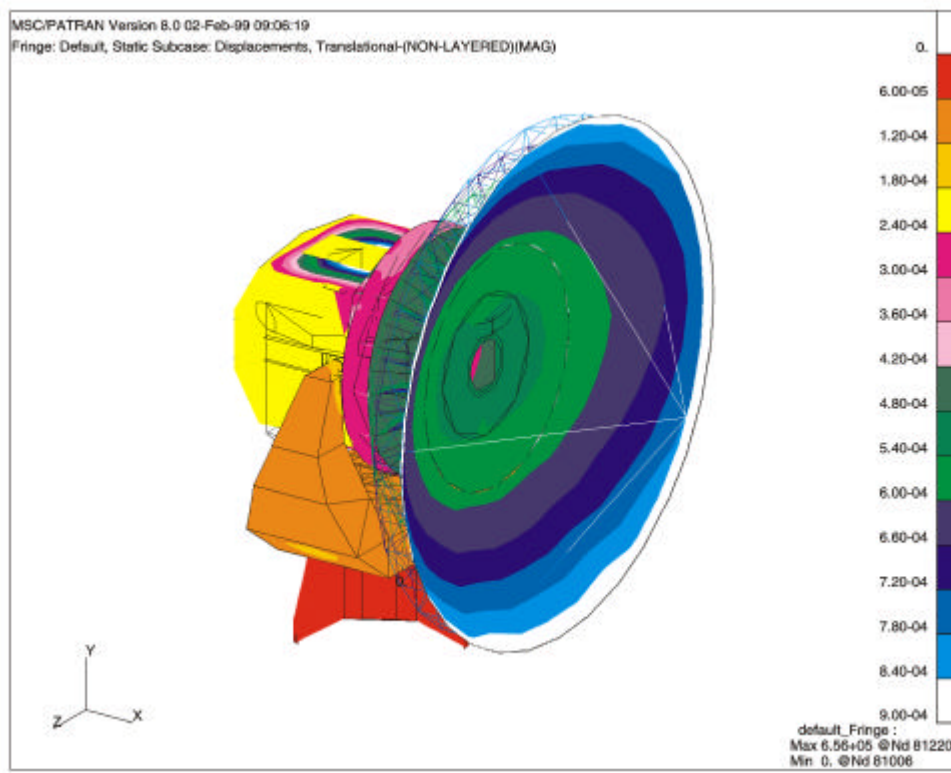


Figure 5.2.3-4. Horizon wind pointing deflection.

The calculation of the wind pointing is done in two parts: a) calculation of the dish response and b) calculation of the yoke and base response. For the dish calculation, the pressure distribution and other wind loads are applied to the model of the dish and cabin with the elevation drive point being fixed. The displacement of the best fit paraboloid plus displacement of secondary mirror grid points are used to calculate the primary beam deviation [22]. For the yoke and base calculation, the wind forces are applied to the complete structure model. Table 5.2.3-1 lists the results for a wind velocity of 9 m/s with the mount metrology system active. We assume the tiltmeters correct the tilt at the azimuth bearing with 90% accuracy.

	Zenith Pointing	Horizon Pointing
Dish	-1.22	-0.01
Mount	-0.13	0.39
Total	-1.35 arc sec	0.38 arc sec

Table 5.2.3-1. Wind pointing results.

The wind induced surface error is very small.

For checking the stress level in survival conditions, a wind velocity of 65 m/sec was used with the dish pointing directly into the wind. A preliminary analysis showed no significant problems.

5.2.4 THERMAL LOAD

Thermal loading on an antenna is difficult to predict. It is a function of antenna pointing, position of the sun, cloud condition, wind direction, wind velocity, and the structure's initial temperature. In the past ten years, a number of temperature measurements have been done on millimeter antennas [8] [14] [15]. However, these measurements only provide statistical data, which are difficult to apply in thermal loading calculations. In this report, four cases of thermal loadings are assumed. The surface change and pointing errors are calculated for each case, as shown in Figures 5.2.4-1 to 5.2.4-8.

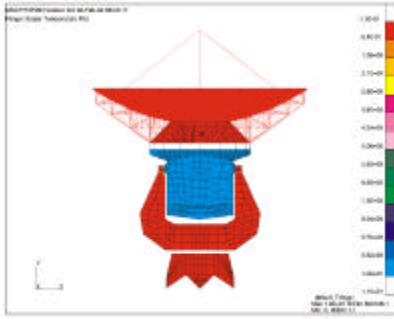


Figure 5.2.4-1. Condition 1.

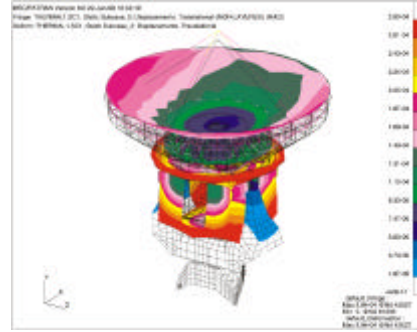


Figure 5.2.4-5. Resultant Deflection Case 1.

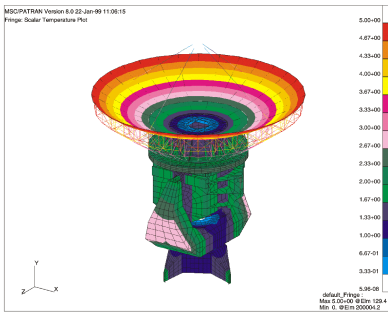


Figure 5.2.4-2. Condition 2.

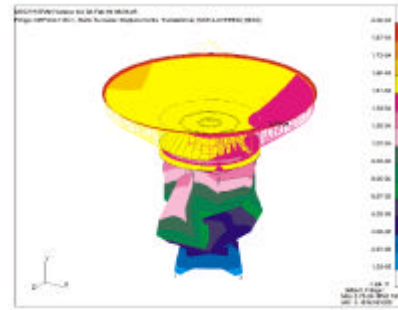


Figure 5.2.4-6. Resultant Deflection Case 2.

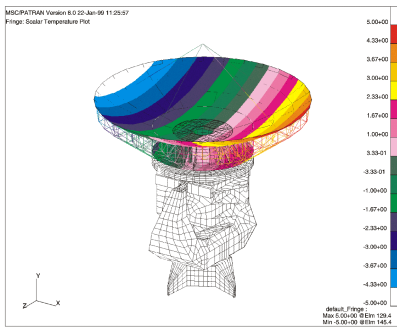


Figure 5.2.4-3. Condition 3.

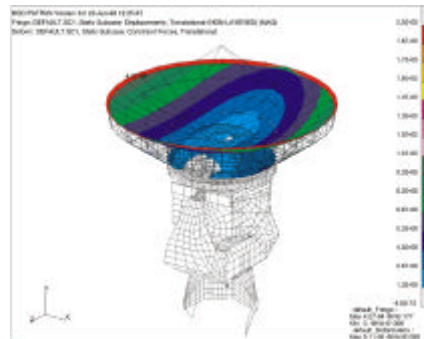


Figure 5.2.4-7. Resultant Deflection Case 3.

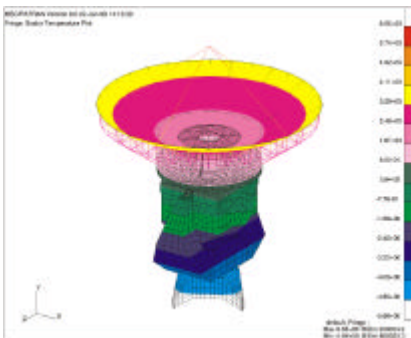


Figure 5.2.4-4. Condition 4.

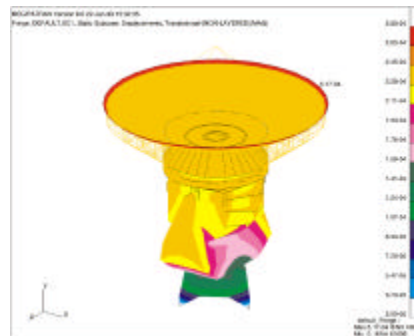


Figure 5.2.4-8. Resultant Deflection Case 4.

In the first thermal case, the cabin temperature is 10 C above the rest of the structure. In the second case, the temperature increases radially 1 C/m. In the third case, the temperature increases along the x-direction at the gradient of 1 C/m. In the last case, the temperature increases along the y-direction at the gradient of 1 C/m. The results are listed in Table 5.2.4-1. In case 1a), the flexures joining the BUS to cabin have 3 mm thickness, and in 1b), the flexures have a 1 mm thickness.

Thermal Case	Surface error	Pointing Error
Case 1a	14.7 μm rms	-0.283 arc sec
Case 1b	9.4 μm rms	-0.707 arc sec
Case 2	1.0 μm rms	0.524 arc sec
Case 3	0.07 μm rms	0.256 arc sec
Case 4	0.12 μm rms	-0.241 arc sec

Table 5.2.4-1. Thermal Pointing and Surface Errors.

5.2.5 PATH LENGTH ERRORS

Path length errors occur when the dish surface has axial movement. Gravity, thermal, dynamic, and wind loadings all produce path length errors. However, because the gravity error is repeatable and common to all antennas, it has no effect. Only non-repeatable errors, caused by wind and thermal loading, need careful study. The path length error with the dish facing directly into 9 m/s wind is 26 μm with the metrology system inactive, and about 6 μm with the metrology system active.

5.2.6 MODAL ANALYSIS

The lowest modes of vibration are limiting factors in the antenna dynamic performance. These modes limit the obtainable bandwidth of the control system and are a measure of the stiffness of the structure and the stability of the antenna with respect to disturbances.

The lowest resonant frequency is 9.01 Hz, which is lateral bending of the yoke arms and cabin walls (see Figure 5.2.6-1). This mode is an effect of long yoke arms and a large receiver cabin. In principle this mode is not excited by either elevation or azimuth drives. The second mode is 9.29 Hz torsional about the azimuth axis. An improvement could be made by increasing azimuth drive stiffness. The next mode is 10.21 Hz about the elevation axis as shown in Figure 5.2.6-3. This could also be improved by increasing elevation drive stiffness.. The fourth mode is a local effect of the cabin top. The fifth mode is the feedlegs in torsional mode as shown in Figure 5.2.6-5. The locked rotor resonance frequency performance is among the best for this antenna diameter as shown in Appendix B by Pidhayny and Andersen [23].

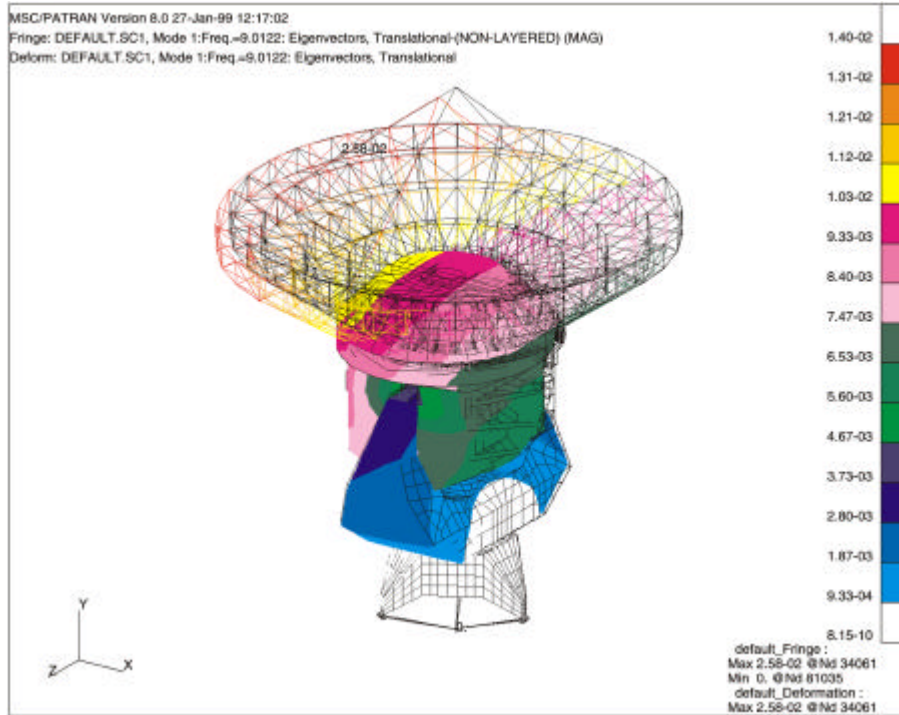


Figure 5.2.6-1. Mode 1.

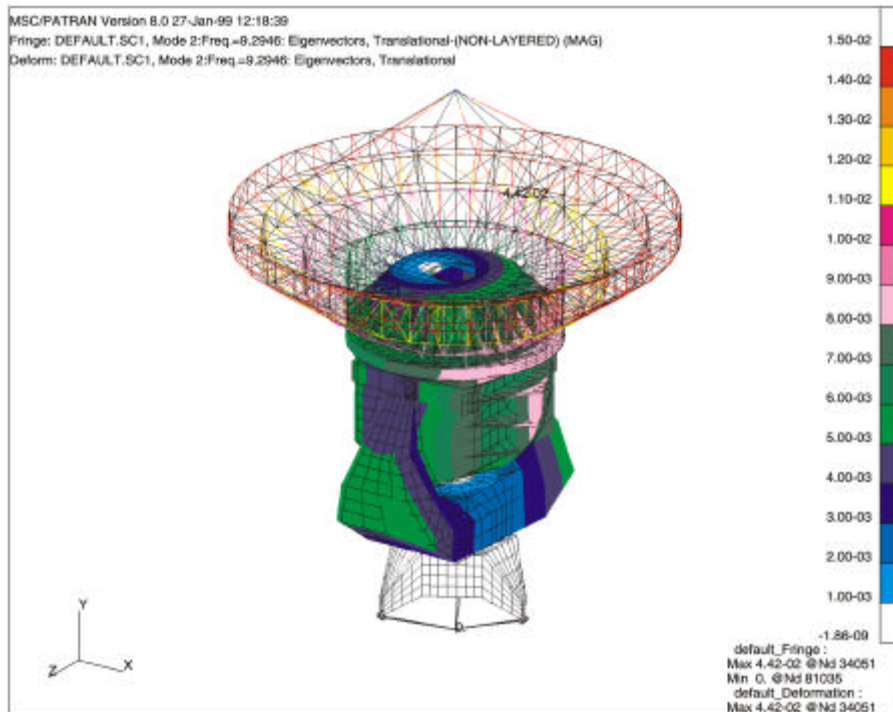


Figure 5.2.6-2. Mode 2.

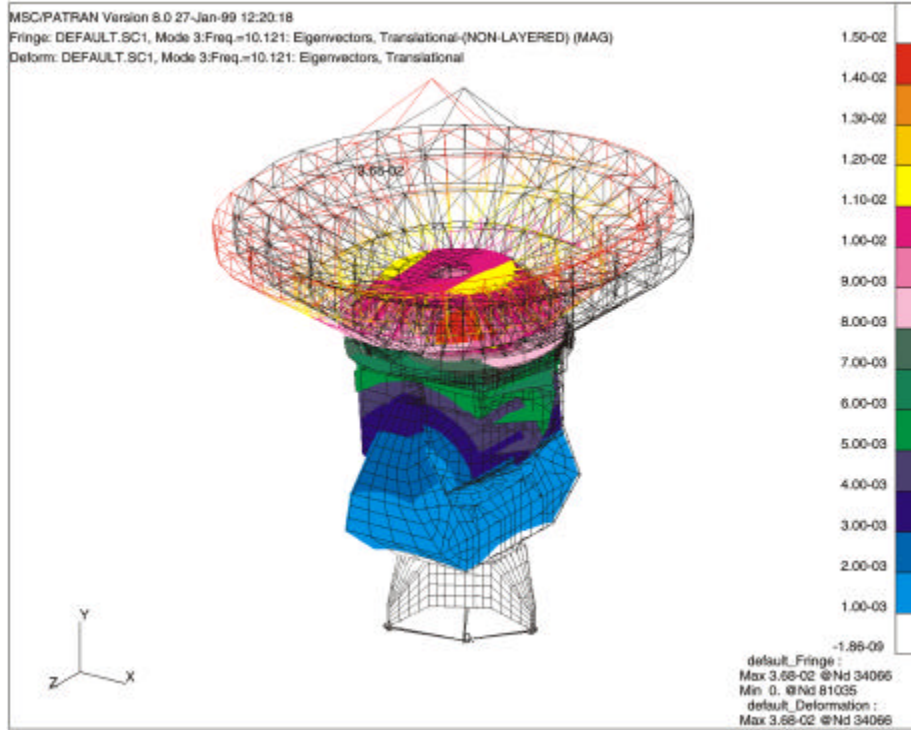


Figure 5.2.6-3. Mode 3.

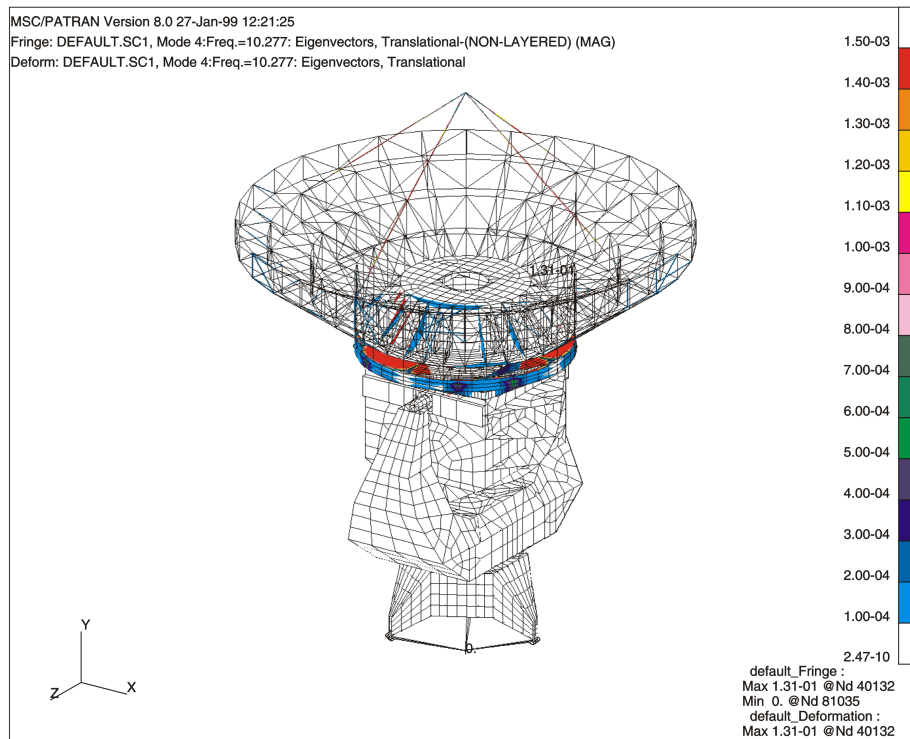


Figure 5.2.6-4. Mode 4.

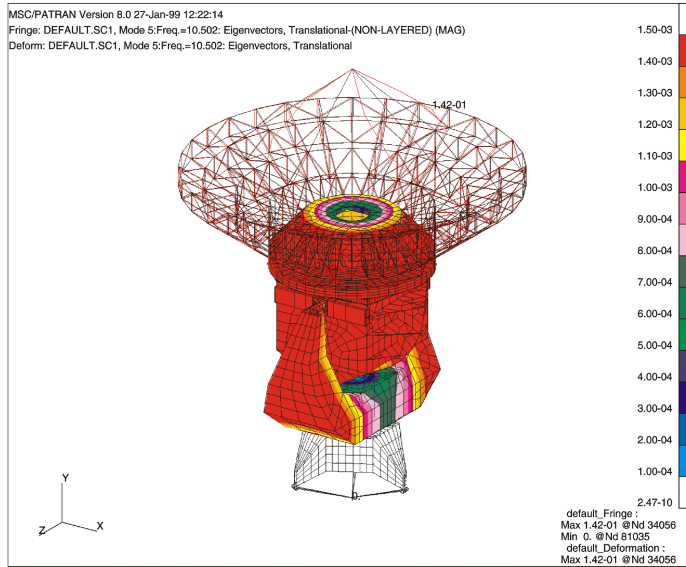


Figure 5.2.6-5. Mode 5.

	Frequency(Hz)	Mode shape
Mode 1	9.01	Cabin along elevation axis
Mode 2	9.29	Around azimuth axis
Mode 3	10.12	About elevation axis
Mode 4	10.28	Cabin top local
Mode 5	10.50	Feedleg rotation

Figure 5.2.6-6. Summary of modal analysis.

5.2.6 DYNAMIC PERFORMANCE

To estimate the likely dynamic performance of the antenna, a very simplified model of the antenna and drives was made. It consists of a lumped mass with the rotational inertia of the antenna, a second lumped mass with the equivalent inertia of the drive motor, and a single torsional spring between the two having the appropriate stiffness to reproduce the lowest locked rotor resonant frequency of the complete antenna model. The simple model assumes essentially infinite stiffness between the drive motor and antenna foundation and attributes all the antenna compliance to the drive. Although crude, this simple dynamical model can give some idea of the antenna servo performance.

The performance of several possible servo systems using this simple model has been studied in MMA Memo #230 [24]. In addition to that work, the open-loop response of the simple model has been studied for a set of smooth forcing functions, in particular $(\sin(t))^n$ for $n = 2$ and $n = 3$. The open loop response of the simple model appears to be adequate with a locked rotor resonant frequency as low as 6 Hz. The actual lowest resonant frequencies of the antenna about the azimuth and elevation axes are 9.29 Hz and 10.12 Hz respectively.

6. ANTENNA HANDLING

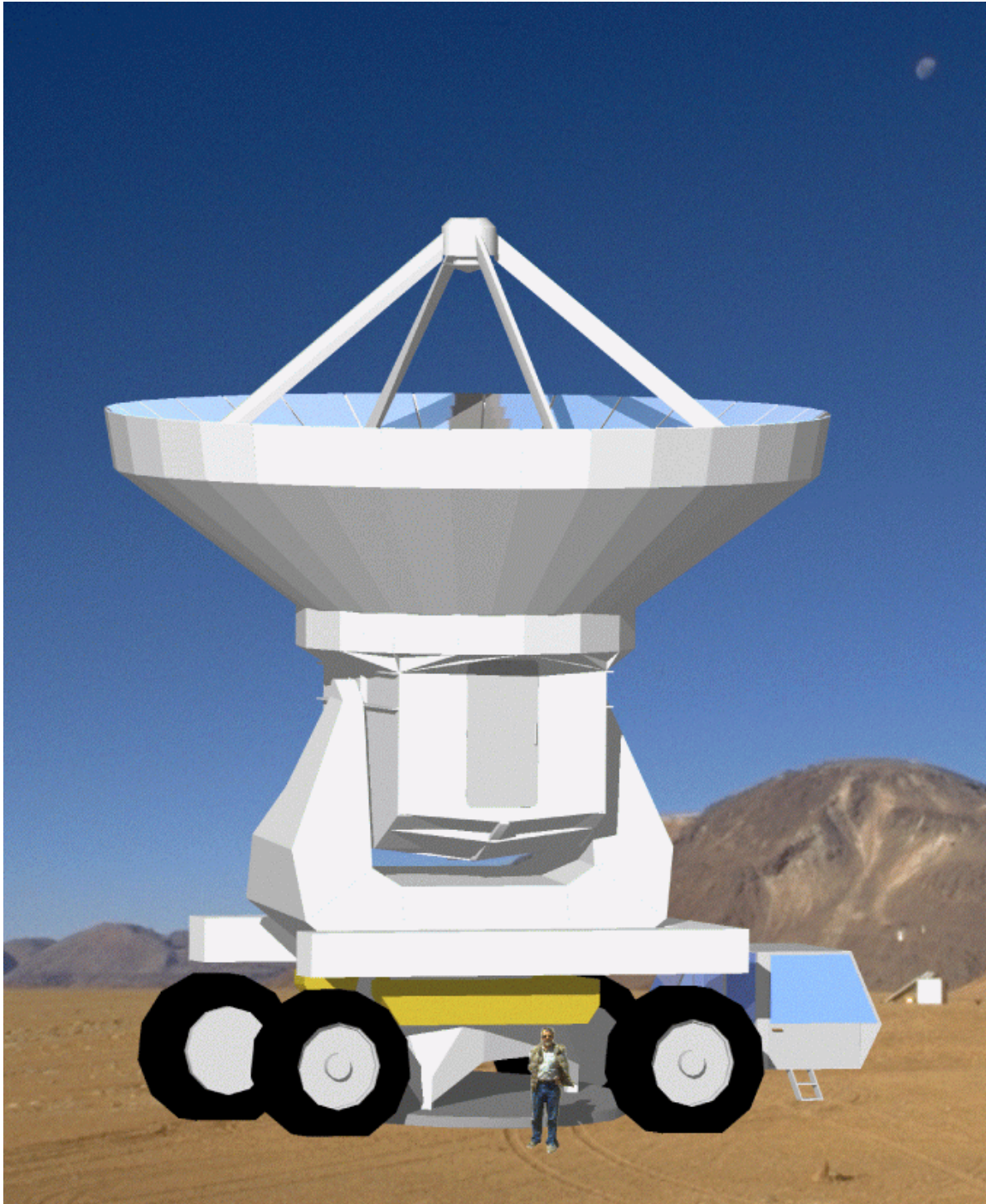


Figure 6.1-1. Antenna transporter side view.

6.1 TRANSPORTER

One of the few factors which was allowed to significantly compromise the antenna design was the need for easy and fast transportability of the antenna [25]. To achieve safe transportability, the transporter (Figures 6.1-1 and 6.1-2) was designed to have a wider footprint than the antenna to foundation interface, so even with a rubber-tired transporter the antenna remains very stable. The antenna base was made more compact than it otherwise would have been in order to keep the transporter overall width to about 5 meters.

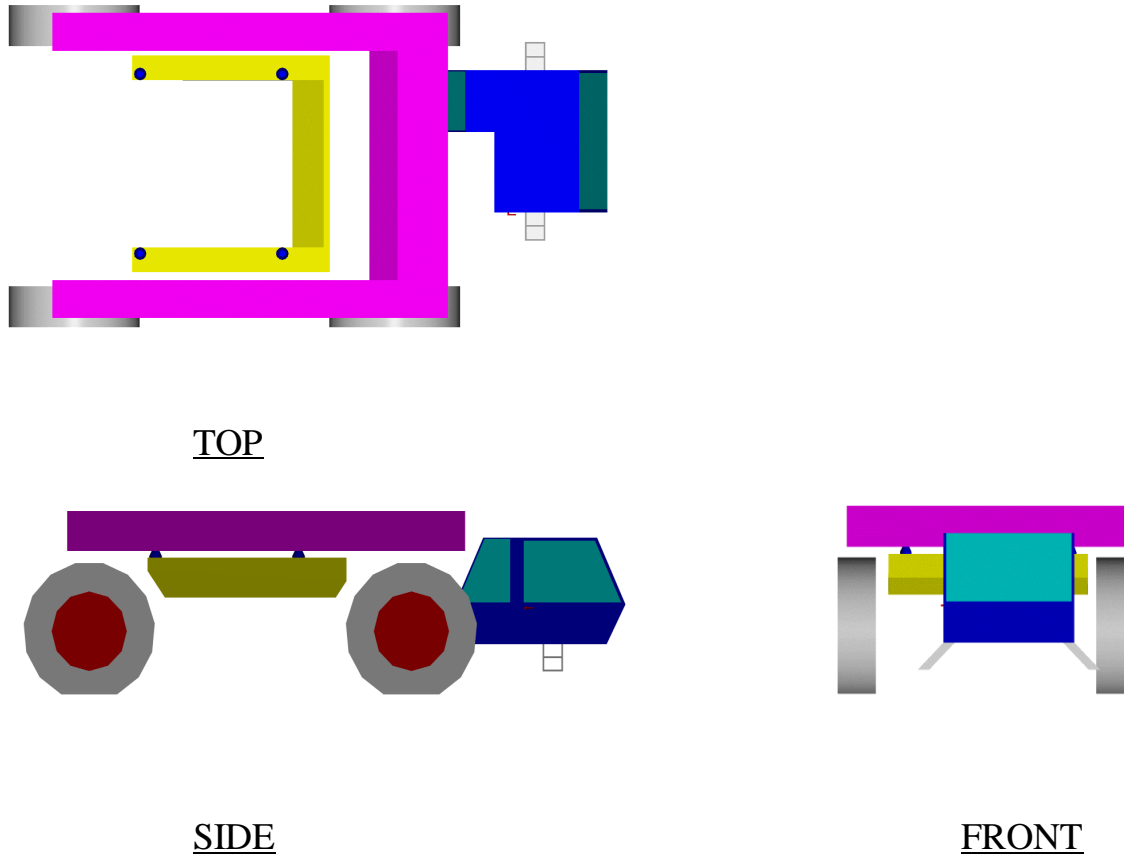


Figure 6.1-2. Transporter views.

The transporter is designed with four large, powered wheels, all of which are steerable, giving it a centerline turning radius of 10 m, which is nearly essential for maneuvering antennas in our compact configurations [26] (Figure 6.1-3). Tire sizes are large enough to give ground bearing pressures that are low enough for traveling on unimproved roads. The vehicle has a comfortable, heated, oxygen-enriched cabin, and simple systems which can be operated by two persons. It contains an auxiliary generator to power the antenna cryogenics and monitoring systems while the antenna is being transported.

To achieve rapid pickup and placement of an antenna, the antenna is lifted by a sub-frame on the transporter which can be shifted by about 10 cm in any direction to easily align the antenna with its new foundation. The antenna is lifted by its yoke, which allows the azimuth bearing to be rotated to align the base with its new foundation. The operator has dual controls which allow forward-facing operation while driving along a road, but rear-facing operation with a good view of the antenna, while maneuvering an antenna onto a new foundation.

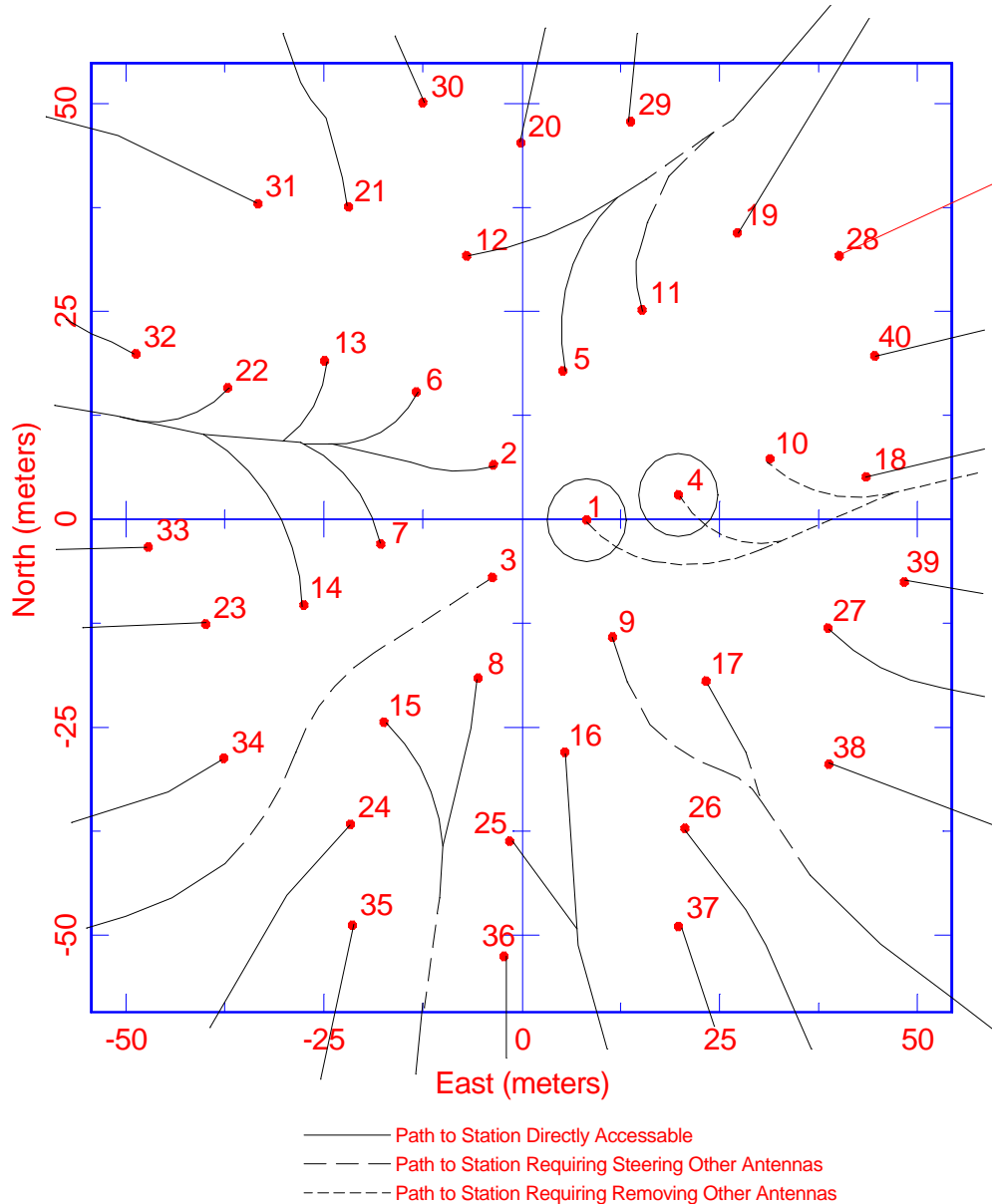


Figure 6.1-3. Sample compact array configuration [26].

6.2 ANTENNA SERVICE VEHICLES

The antenna service vehicles will include receiver service trucks (Figure 6.2-1), boarding stair trucks, maintenance stands, and man-lifts.

The receiver service trucks will have a scissor-lift box on the back. The box will be outfitted with test equipment and tools required for installing, maintaining, and removing the receivers. The box and cab will be oxygen enriched and heated to allow for comfort of the personnel while performing their duties.

The boarding-stair truck will be for accessing the receiver cabin when a receiver service truck is not required.

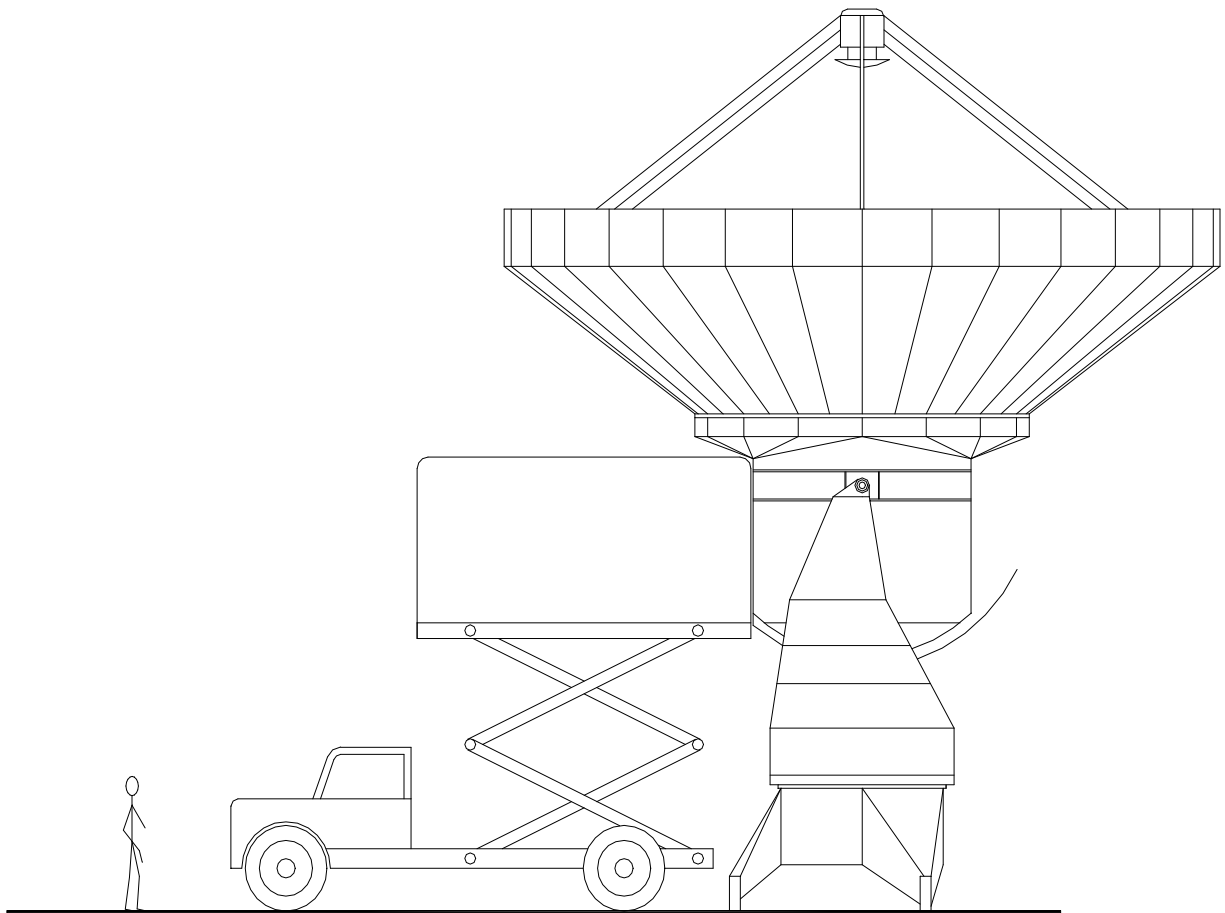


Figure 6.2-1. Receiver service truck.

6.3 ASSEMBLY AND MAINTENANCE FACILITIES

Assembly and maintenance facilities will need to be built at the MMA site and at the San Pedro de Atacama base site. Maintenance facilities at the high site will include an antenna barn for antenna maintenance. When practical, maintenance will be performed at the more hospitable facilities at the base site.

7. CONCLUSIONS

The design presented here is believed to meet the pointing, surface accuracy, and path length stability goals for a 10-meter diameter antenna for the Millimeter Array. It attempts to do so at a low cost and with minimal risk. Some novel approaches are used to meet the performance goals cost effectively - for example, the use of a non-load bearing reference structure to achieve the desired pointing accuracy. However, these steps forward are undertaken as conservatively as possible, using untried ideas, unusual materials, or unconventional construction techniques as little as possible. Taking the reference structure as an example; it has no moving parts, it is rigidly attached to structural elements of the telescope, and the displacement sensors only need to measure with a precision of about 1 micron. Although the function of the reference structure package may be new, each element of it is very routine.

While the antenna performance has not been compromised to unacceptable levels, consideration has been given to the needs of integrating the antenna into the entire Millimeter Array instrument. Areas of compromise which did affect the antenna performance were limited mainly to providing a very large and usefully shaped receiver cabin and to designing the interfaces to the transporter and foundation to allow rapid and easy relocation of the antenna to a new foundation using a transporter of reasonable size and weight.

The design presented here has been optimized in some areas, but certainly would benefit from further work. The yoke stiffness-to-weight ratio has not been optimized at all, but is simply a first approximation at this point. Likewise, the cabin structure has not been optimized. A significant increase in the lowest resonant frequencies is likely with these two optimizations. The pointing accuracy near zenith with large wind loads may not meet the desired goal, or does so just marginally, due to insufficient stiffness between the dish, the elevation axles, and elevation encoder. How easily this part of the antenna might be stiffened has not been investigated. Alternatively, a non-load bearing reference structure could be added between the dish and the elevation encoder.

This conceptual design could probably be used for a Millimeter Array antenna as large as 12 m diameter by increasing the mount stiffness and weight. The cabin size would probably remain unchanged. It may be useful to incorporate a reference structure between the elevation encoder and dish. Further optimization of the structure should definitely be undertaken if the design is scaled up.

8. APPENDIX A

ANTENNA DRAWINGS

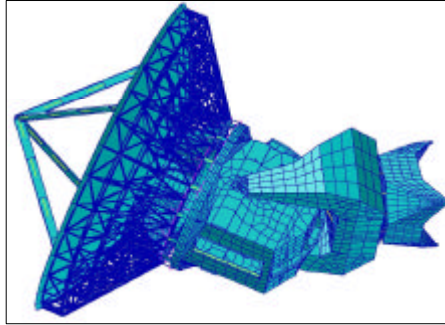
1. Cover Sheet.....	A-1
2. Yoke Design.....	A-2
3. Base Design.....	A-3
4. Receiver Cabin Design.....	A-4
5.Backup Structure Design.....	A-5

MILLIMETER ARRAY

NRAO DESIGN 1

VERSION 1

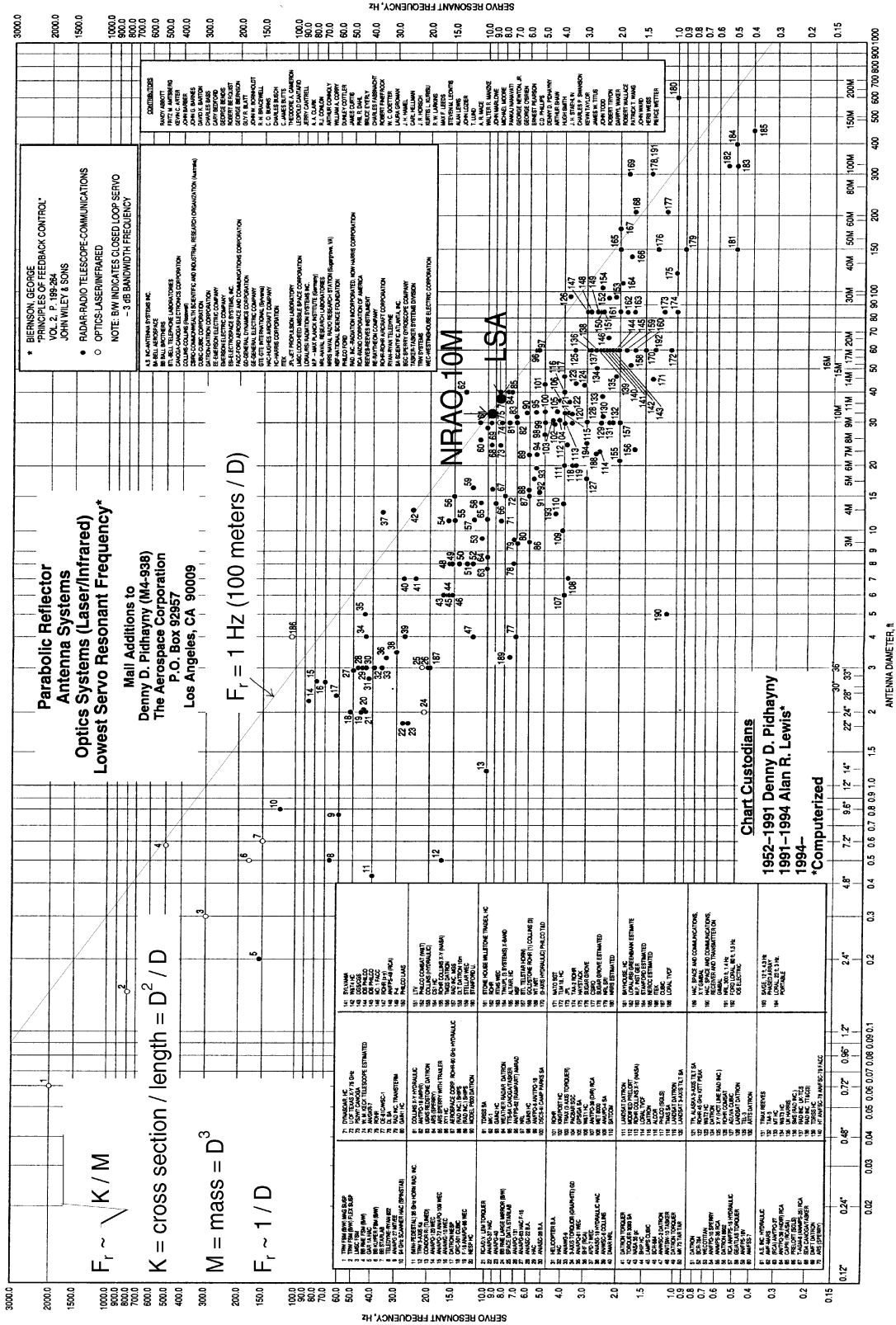
SEPTEMBER 22, 1998



#	DRAWING	DRAWING NO.	FILE
1	YOKE	03010100	YOKE2.DWG
2	BASE	03010101	BASE2.DWG
3	RXCABIN	03010102	RXCABIN.DWG
4	BUS	03010103	BUS.DWG

9. APPENDIX B: LOCKED ROTOR RESONANCE FREQUENCIES

Radar-Radio Telescope-Communications (release January 1994)



11. ACKNOWLEDGMENTS

We want to thank the MMA Antenna Working Group, chaired by Peter Napier, for many useful discussions. Dave Woody, James Lamb, Torben Andersen and Dietmar Plathner have provided many stimulating ideas and useful discussion, which have benefitted this antenna design. Mark Holdaway has provided valuable guidance in determining the performance requirements for the antenna. Simon Radford first suggested the idea of a scissors lift for the receiver service truck. John Lugten thanks the Radio Astronomy Laboratory at U.C. Berkeley for the opportunity to participate in the Millimeter Array project. That work provided much of the basis for this design as it now stands.

12. REFERENCES

- [1] J. Lugten, P. Napier, J. Bieging, J. Cheng, D. Emerson, M. Fleming, M. Holdaway, J. Kingsley, J. Lamb, J. Mangum, J. Payne, W. Welch, D. Woody : “A Strawman Optics Layout for the MMA Antenna -version 2,” NRAO MMA Memo #215 , June 1998.
- [2] J. Lugten, W. Welch : “A suggested Receiver Layout for the MMA Antenna,” NRAO MMA Memo #183, September 1997.
- [3] P. Napier, J. Bieging, J. Cheng, D. Emerson, M. Gordon, M. Holdaway, J. Kingsley, J. Lugten, J. Payne, D. Woody : “A Strawman Optics Layout for the MMA Antenna,” NRAO MMA Memo #163 , November 1996.
- [4] J. W. Lamb: “Spillover Control on the Secondary Mirror Struts,” NRAO MMA Memo #195, January 1998.
- [5] J. B. Lugten, W. J. Welch, J. L. Gibson: “Antenna Noise in the Berkeley-Illinois-Maryland Array,” URSI National Radio Science Meeting, J1-4 14440, January 1996.
- [6] J. Cheng & J. Mangum: “Feed Leg Blockage and Ground Radiation Pickup for Cassegrain Antennas,” NRAO Memo #197, February 1998.
- [7] J. Cheng: “Visit to SMA and Bosma,” NRAO MMA Memo #132, May 1995.
- [8] J. W. Lamb: “Thermal Considerations for MMA Antennas,” NRAO MMA Memo #83, May 1992.
- [9] J. Lugten, J. Cheng, M. Fleming, J. Kingsley: “Antenna design for the Millimeter Array,” SPIE 1998 Symposium on **Astronomical Telescopes and Instruments** (Conference 3357: Advanced Technology MMW, Radio, and Terahertz Telescopes), March 20-28 1998.
- [10] M. Fleming: “Discussion of Drives and Axis Bearings for MMA Antennas.” NRAO Memo #244, February 1999.
- [11] IGUS, Inc., P.O. Box 14349, East Providence, RI 02914-0349, USA (800) 521-2747.
- [12] J. B. Lugten: “A Simple Method to Improve Pointing on the MMA Antennas,” NRAO Memo #232, October 1998.
- [13] Applied Geomechanics Inc., 1336 Brommer Street, Santa Cruz, CA 95052, USA (408) 462-4418.
- [14] J. Lamb & D. Woody: “Thermal Behavior of the Leighton 10-m Antenna Backing Structure,” NRAO Memo #234, October 1998.
- [15] J. Cheng: “Thermal Behavior of BIMA Antenna Dish Structure,” NRAO Memo #141, September 1995.

- [16] J. M. Payne: "Notes on Possible Sensors for Improving the Pointing of MMA Antennas," NRAO MMA Memo #181, August 1997.
- [17] MSC/Patran Version 8.0, The MacNeal-Schwendler Corporation, 815 Colorado Boulevard, Los Angeles, CA 90041-1777.
- [18] MSC/NASTRAN Version 70, The MacNeal-Schwendler Corporation, 815 Colorado Boulevard, Los Angeles, CA 90041-1777.
- [19] Levy, R., *Structural Engineering of Microwave Antennas: For Electrical, Mechanical, and Civil Engineering*, IEEE Press, New York, NY, 1996, pp. xx-xx
- [20] Fox N., "Load Distribution on the Surface of Paraboloid Reflector Antennas," Aerodynamic Facilities Section 373, Internal Memorandum CP-4, JPL, Pasadena, CA, July 1962, JPL
- [21] M.A. Holdaway, D. Emerson, J. Cheng, F. Schwab: "Wind Velocities at the Chajnantor and Mauna Kea Sites and the Effects on MMA Pointing," NRAO MMA Memo #159, August 1996.
- [22] J. Ruze: "Small Displacements in Parabolic Reflectors," unpublished paper, MIT Lincoln Laboratory, Lexington, Massachusetts, February 1969.
- [23] T. Andersen: "Feasibility Study for a 12 m Submillimeter Antenna," ESO Report, September 1997.
- [24] T. Andersen: "A First Study of MMA Antenna Offset Performance," NRAO Memo #230, October 1998.
- [25] M. A. Holdaway, F. N. Owen: "How Quickly Can the MMA Reconfigure?," NRAO MMA Memo #147, February 1996.
- [26] M. A. Holdaway: "Evaluating the MMA Compact Configuration Designs," NRAO MMA Memo #81, March 1992.